Linda A. Hinnov and Andrea Cozzi, 2020. Rhaetian (Late Triassic) Milankovitch Cycles in the Tethyan Dachstein Limestone and Laurentian Passaic Formation Linked by the g_2-g_5 Astronomical Metronome. Boletín Geológico y Minero, 131 (2): 269-290
ISSN: 0366-0176
DOI: 10.21701/bolgeomin.131.2.004

Rhaetian (Late Triassic) Milankovitch Cycles in the Tethyan Dachstein Limestone and Laurentian Passaic Formation Linked by the g_2-g_5 Astronomical Metronome

Linda A. Hinnov[(1)] and Andrea Cozzi[(2)]

(1) George Mason University, Fairfax, Virginia, USA 22030.
(2) Eni SpA, Via Emilia 1, 20097 San Donato Milanese, Italy.

ABSTRACT

Milankovitch cycles have long been suspected of having been recorded in the shallow marine Lofer cyclothems of the Rhaetian Dachstein Limestone of the European Northern and Southern Calcareous Alps. However, sufficient evidence has not yet been forthcoming to make a compelling case for Milankovitch control on the cyclothems. At the same time, there is overwhelmingly strong evidence that Milankovitch cycles were influencing the paleoclimates of Rhaetian Laurentia and the wet-dry playa lake deposits of the Passaic Formation (Newark Basin, USA). The strongest cycles in these deposits, the McLaughlin cycles, have been linked to the metronomic g_2-g_5, or 405 kyr orbital eccentricity cycle. Thus, Milankovitch cycles were operating throughout the Rhaetian, and being global in nature, likely played a role in the genesis of the coeval Lofer cyclothems. The Dachstein Limestone in the Julian Alps, relatively undisturbed by tectonics, exhibits strong Milankovitch-like cyclicity, including evidence for g_2-g_5 cycling. The shallow marine Dachstein and continental Passaic formations provide evidence for complementary forcing mechanisms and active aquifer-limno-eustasy: low sea level in Lofer exposure facies is reflected in wet Passaic playa lake deposits, and high sea level in Lofer subtidal facies in dry Passaic playa lake deposits. The Dachstein and Passaic formations are further linked by the g_2-g_5 metronome; a provisional correlation is proposed, subject to future validation by additional, as yet undeveloped chronostratigraphic constraints.

Keywords: Lofer cyclothems, Julian Alps, Newark Basin, cyclostratigraphy, Triassic.

Ciclos de Milankovitch del Rhaetiense (Triásico Superior) en las formaciones Tethyan Dachstein Limstone y Laurentian Passaic Formation vinculadas por el metrónomo astronómico g_2-g_5

RESUMEN

Se ha venido sospechando desde hace mucho que los ciclos de Milankovitch se han registrado en los ciclotemas Lofer correspondientes a un ambiente marino somero de la Rhaetian Dachstein Limestone de las zonas norte y sur de los European Northern and Southern Calcareous Alps. Sin embargo, la evidencia no ha sido todavía suficiente para demostrar de modo inequívoco el control de Milankovitch sobre los ciclotemas. Al mismo tiempo, hay una evidencia abrumadoramente fuerte de que los ciclos de Milankovitch influenciaron los paleoclimas de Rhaetian Laurentia y los depósitos húmedo-seco de playa-lake de la Passaic Formation (Newark Basin, USA). Los ciclos más claros en estos depósitos, los ciclos McLaughlin, se han asociado al metrónomo g_2-g_5, o ciclo orbital de excentricidad de 405 ka.

De este modo, los ciclos de Milankovitch estuvieron operando a lo largo del Rhaetiense, y siendo de naturaleza global, es muy factible que jugaran un papel en la génesis de los ciclotemas Lofer coetáneos. La Dachstein Limestone en los Julian Alps, relativamente no muy alterados por la tectónica, exhiben una fuerte ciclicidad de tipo Milankovitch, incluyendo evidencia de ciclicidad g_2-g_5. La formación marina somera Dachstein y la continental Passaic proporcionan evidencia para mecanismos complementarios de impulso y acuífero-limno-eustasia activa: el nivel del mar bajo en las facies emergidas Lofer es un reflejo de los depósitos Passaic húmedos de playa-lake, y nivel del mar alto en las facies subtidales Lofer en depósitos Passaic de playa-lake secos. Las formaciones Dachstein y Passaic están además asociadas por el metrónomo g_2-g_5; se propone una correlación provisional, sujeto a una validación futura con adicional, aunque todavía no desarrolladas restricciones cronoestratigráficas.

Palabras clave: ciclotemas Lofer, Alpes julianos, Cuenca Newark, cicloestratigrafía, Triásico

Introduction

More than seventy years ago, Walther Schwarzacher launched a groundbreaking initiative in 20th century stratigraphy, namely, quantitative research into the origins of ancient sedimentary cycles, with the publication of his 1947 paper "Über die sedimentäre Rhytmik des Dachstein Kalkes von Lofer." (Schwarzacher, 1947). This seminal publication inspired numerous subsequent investigations into the anatomy of the "Lofer cyclothems" of the Upper Triassic Dachstein Limestone at locations throughout the Alpine and Trans-Danubian provinces, in the effort to explain the origin of the rhythmic stratification (Table 1). Similarly, the extensive rhythmic stratal sequences in the Southern Alps leading up to the Dachstein Limestone have also garnered detailed scientific scrutiny, including the Anisian Latemar Limestone (e.g., Goldhammer et al., 1987; Egenhoff et al., 1999; Preto et al., 2001, 2004; Zühlke, 2004), the Carnian Dürrenstein Formation (Preto and Hinnov, 2003), and the late Carnian-Norian Dolomia Principale (Forkner, 2007; Caggiati et al., 2017).

While a number of problems have been resolved over the years, the fundamental question about the cause of the rhythmicity has never been satisfactorily answered, and the origin of cyclic stratification of the peritidal Dachstein Limestone remains contested. In particular, were the Lofer cyclothems produced by sea level oscillations forced by Milankovitch cycles, or do they reflect autocyclic processes inherent to carbonate platform evolution? Are the Lofer cyclothems transgressive, regressive, or both, and what is the significance of the attribution in terms of sea level oscillations? Another problem is that most of the Dachstein-Lofer studies have thus far been conducted in the Northern Calcareous Alps, where tectonics has severely fragmented the Triassic section. By contrast, in the Southern Calcareous Alps, the Dachstein is relatively undisturbed. For example, in the Julian Alps of northeastern Italy, stacks of platform carbonate cycles that are many hundreds of meters thick crop out in spectacular mountainous settings (Cozzi et al., 2005). Here, the meter-scale Lofer cyclothems are clearly stratigraphically bundled into groups of 5-6; these bundles in turn are super-bundled into groups of ~4. This is a hallmark of Milankovitch forcing in cyclostratigraphy.

While the role of Milankovitch forcing of the Lofer cyclothems of Tethys has not been confirmed with confidence, a very different conclusion has been reached for the coeval continental deposits of the Newark Basin, eastern North America. These thick, rift-basin de-

Publication	**Locality/Localities**
Sander (1936)	Loferer and Leoganger Steinberge, Steinbruch Golling, Buchstein, Dachstein, Wetterstein; Northern Calcareous Alps
Schwarzacher (1947)	Loferer Steinberge; Northern Calcareous Alps
Schwarzacher (1954)	Loferer Steinberge; Northern Calcareous Alps
Fischer (1964)	Loferer and Leoganger Steinberge, Steinernes Meer, Dachstein; Northern Calcareous Alps
Haas (1982, 1991, 1994, 2002)	Transdanubian Range, Hungary
Goldhammer et al. (1990)	Steinernes Meer; Northern Calcareous Alps
Satterley and Brandner (1995) Satterley (1996)	Steinernes Meer, Hochkönig Massif; Northern Calcareous Alps
Balog et al. (1997, 1999)	Transdanubian Range, Hungary
Enos and Samankassou (1998)	Steinernes Meer; Northern Calcareous Alps
Schwarzacher (2005)	Loferer, Leogang and Steinernes Meer; Northern Calcareous Alps
Cozzi et al. (2005)	Monte Canin, Julian Alps; Southern Calcareous Alps
Pomoni-Papaionnou (2008)	Pelagonian Zone, Greece
Haas et al. (2009)	Transdanubian Range, Hungary; Pelagonian Zone, Greece
Samankassou and Enos (2017, 2018)	Steinernes Meer; Northern Calcareous Alps

Table 1. Key studies on the Dachstein Limestone and the Lofer cyclothems.
Tabla 1. *Estudios más relevantes sobre las Dachstein Limestone y los ciclotemas Lofer.*

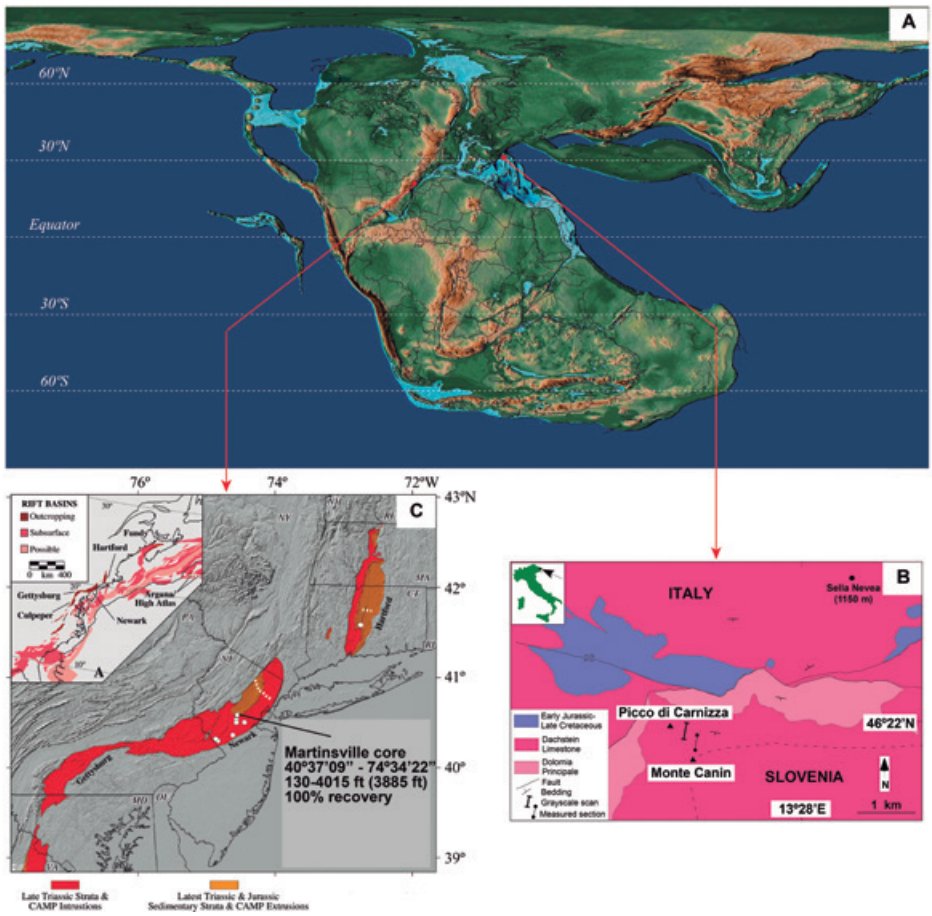

Figure 1. Rhaetian marine and continental study areas. A. End-Triassic paleogeography (modified from Scotese, 2013). B. Dachstein Limestone, Picco di Carnizza at Monte Canin, Julian Alps, Italy (from Cozzi et al., 2005). C. Passaic Formation, Martinsville Core, Newark Basin, New Jersey, USA (from Olsen et al., 2011).

Figura 1. *Áreas de estudio marinas y continentales del Rhaetiense. A. Paleogeografía del final del Triásico (modificada de Scotese, 2013). B. Dachstein Limestone, Picco di Carnizza en Monte Canin, Julian Alps, Italia (de Cozzi et al., 2005). C. Passaic Formation, Martinsville Core, Newark Basin, New Jersey, EEUU (de Olsen et al., 2011).*

posits have long been known for their predominant and systematic cycling between deep lake to lake margin environments in a three-tiered hierarchical pattern that was first described and attributed to precessional forcing by Van Houten (1962, 1964). The Milankovitch forcing signal was subsequently greatly clarified by 7 km of drill-core taken through the entire ~30 million year-long sequence with efforts to develop independent chronstratigraphic constraints that have continued up to the present day (e.g., Olsen and Kent, 1996; Olsen et al., 1996; Olsen and Kent, 1999; Olsen et al., 2011; Kent et al., 2017, 2018; Olsen et al., 2019).

Here, available cyclostratigraphic proxies from the Dachstein upper member from Cozzi et al (2005) and the upper Passaic Formation of the Martinsville core from Olsen and Kent (1996) are reanalyzed to address the following questions:

- Are there astronomical frequencies in these proxies?
- Does minimal tuning align astronomical frequencies?
- What is the astrochronological duration of the Rhaetian?
- Is there evidence for the g_2-g_5 metronome in the Dachstein?
- Do these marine-continental proxies indicate limno-aquifer-eustasy?

Data

Geological Setting and Time Constraints

During the Late Triassic Period, the supercontinent Pangaea began to rift along its central zone from Greenland and Europe in the northeast to the Gulf of Mexico and the Pacific Ocean in the southwest (Figure 1A). The region occupied today by eastern North America was characterized by half-grabens and lakes with dimensions comparable in size to the North American and East African Great Lakes (Letourneau

A.

Model #	Geologic time (Ma)	Precession frequency k (arcsec/year)	Length-of-day (hours)	Earth-Moon distance (km)
0	0	50.475838	24.0	384000
1	200	56.625189	22.41	376452
2	200	53.775930	23.23	379200

B.

Fundamental frequency	Value (0-5 Ma) in arcsec/year
g_2	7.452
g_3	17.368
g_4	17.916
g_5	4.257452
s_6	-26.347855
s_3	-18.850
s_4	-17.755
s_2	-7.05

Table 2. Variables used to calculate the astronomical parameter periodicities for three models. A. Model 0 represents the present-day values for k, length-of-day (LOD) and Earth-Moon distance; Model 1 is from Equation 39 (for Earth-Moon distance), Equation 40 (for k, denoted as "p-") and Equation 41 (for "LOD-") in Laskar et al. (2004) evaluated at-200 Myr; and Model 2 is from the Milankovitch Calculator of Waltham (2015) set to 200 Ma. B. Fundamental frequencies for the orbits of Venus (subscript 2), Earth (subscript 3), Mars (subscript 4), Jupiter (subscript 5), and Saturn (subscript 6) that contribute to the obliquity and precession index cycles.

Table 2. *Variables usadas para calcular los parámetros de periodicidades astronómicas para tres modelos. A. El Modelo 0 representa los valores actuals para k, duración del día (LOD) y distancia Tierra-Luna; el Modelo 1es de la ecuación 39 (para la distancia Tierra-Luna), ecuación 40 (para k, denotado como "p-") y ecuación 41 (para "LOD-") en Laskar et al. (2004) evaluado a -200 Ma; y el Modelo 2 es de la calculadora de Milankovitch de Waltham (2015) ajustado a 200 Ma. B. Las frecuencias fundamentals para las órbitas de Venus (subíndice 2), la Tierra (subíndice 3), Marte (subíndice 4), Jupiter (subíndice 5), y Saturno (subíndice 6) que contribuyen a los índices de los ciclos de oblicuidad y precesión.*

and Olsen, 2003; Withjack et al., 2012, 2013). Ultimately, the rifting led to the formation of the North Atlantic Ocean during the Jurassic Period, and continues today along the central Atlantic Ridge. Today, thick sediments of these Triassic-early Jurassic lake systems are found throughout the relict rift margins of eastern North America (Figure 1C) and Morocco. At the same time, the region comprising the present-day Northern and Southern Calcareous Alps of western Europe hosted a broad, shallow marine carbonate platform on the northwestern margin of the Tethys Ocean (e.g., Mandl, 2000; Flügel, 2002). This platform is preserved in the Norian-Rhaetian Dachstein Limestone, with meter-scale peritidal carbonate cycles stacked in hundreds of meters of section, leading up through the Triassic-Jurassic boundary and continuing into the early Jurassic as the Calcari Grigi Formation.

The geochronology of the T-J boundary and the Rhaetian Stage has been the focus of intense study over the past decade. The flood basalts at the top of the Passaic Formation have now been dated and integrated with the Passaic deposits, with a precision that has distinguished an age of 201.564±0.015 Ma for the End-Triassic Extinction (ETE) (Blackburn et al., 2013). In the Pucara Basin of Peru, a slightly younger age was obtained for the Triassic-Jurassic boundary: 201.31±0.18 Ma by Schoene et al. (2010), and 201.36±0.17 Ma by Wotzlaw et al. (2014). The latter also provided an age of 205.50±0.35 Ma for the Norian/Rhaetian boundary, i.e., a duration of 4.14±0.39 Myr for the Rhaetian Stage.

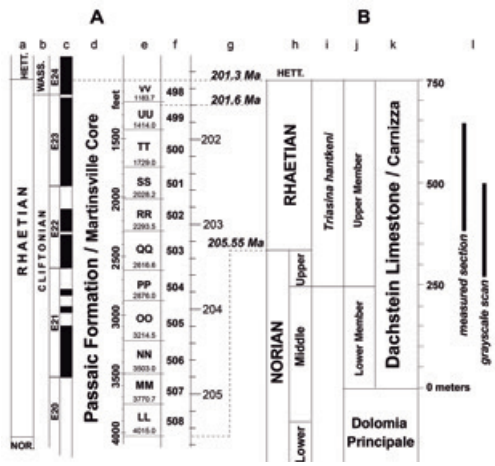

Figure 2. Chronostratigraphic constraints. A. the Martinsville Core, Passaic Formation, Newark Basin, New Jersey, USA. a=Stage; b=Land Vertebrate Age; c=Martinsville magnetic reversal stratigraphy; d=Martinsville core depth (ft); e=McLaughlin cycle (numbers indicate core depth between cycles); f=g_2-g_5 cycle number (see text); g=geologic time scale. B. Monte Canin, Dachstein Limestone, Julian Alps, Italy. h=Stage; i=biostratigraphy, j=Dachstein member; k=formations; l=coverage of grayscale scan (Picco di Carnizza) and measured section (Monte Canin) (see Figure 1B). 201.3 Ma is the age of the Triassic/Jurassic boundary; 201.6 Ma is the time of the End Triassic Extinction; 205.55 Ma is the age of the Norian/Rhaetian boundary (Kent et al., 2017).

Figura 2. *Restricciones cronoestratigráficas. A. la sección Martinsville, Passaic Formation, Newark Basin, New Jersey, USA. a=Piso; b=Edad por vertebrados terrestres; c=estratigrafía de inversion magnética de Martinsville; d=profundidad de la sección Martinsville (ft); e= ciclo McLaughlin (los números indican la profundidad de la sección entre ciclos); f= número del ciclo g_2-g_5 (ver texto); g=escala de tiempo geológico. B. Monte Canin, Dachstein Limestone, Julian Alps, Italy. h=Piso; i=bioestratigrafía, j=miembro Dachstein; k=formaciones; l=zona cubierta por el escaneo de escala de grises (Picco di Carnizza) y sección medida (Monte Canin) (ver Figure 1B). 201.3 Ma es la edad del límite Triásico/Jurásico; 201.6 Ma es la edad de la extinción del final del Triásico; 205.55 Ma es la edad del límite Noriense/Rhaetiense (Kent et al., 2017).*

A.

Parameter	Term	Model 0, 1, and 2 in arcsec/year	Model 0, 1, and 2 in periodicity (year)
long orbital eccentricity	g_2-g_5	3.199279	405091
short orbital eccentricity	g_3-g_2	9.909679	130781
	g_4-g_2	10.456224	123945
	g_3-g_5	13.109803	98857
	g_4-g_5	13.651920	94932

B.

Parameter	Term	Model 0 in arcsec/year	Model 0 in periodicity (year)	Model 1 in arcsec/year	Model 1 in periodicity (year)	Model 2 in arcsec/year	Model 2 in periodicity (year)
obliquity	k+s_6	24.127937	53714	30.277334	42804	27.42808	47251
	k+s_3	31.625837	40979	37.775189	34308	34.92593	37107
	k+s_4	32.720837	39608	38.870189	33342	36.02093	35979
	k+s_2	43.425838	29844	49.575189	26142	46.72593	27736
precession index	k+g_5	54.733288	23678	60.882641	21287	58.03338	22332
	k+g_2	57.927837	22373	64.077189	20226	61.22793	21167
	k+g_3	67.843842	19103	73.993189	17515	71.14393	18217
	k+g_4	68.391838	18950	74.541189	17386	71.69193	18077

Table 3. Astronomical parameters for present-day and Late Triassic models. **A**. Earth's orbital eccentricity is from the La2004 solution (Laskar et al., 2004), adopted for all three models. **B**. Model 0 for present-day parameters and Model 1 at -200 Myr (Laskar et al., 2004); Model 2 according to the Milankovitch Calculator (Waltham, 2015). (Values for k are from **Table 2A**; values for g_i and s_i are from **Table 2B**.)

Tabla 3. *Parámetros astronómicos para modelos actual y del Triásico Superior. A. La excentricidad orbital de la Tierra es de la solución La2004 (Laskar et al., 2004), adoptada para los tres modelos. B. Modelo 0 para parámetros actuals y Modelo 1 para -200 Ma (Laskar et al., 2004); Model 2 de acuerdo a la calculadora de Milankovitch (Waltham, 2015). (Los valores para k son de la Tabla 2A; valores para gi y si son de la Tabla 2B).*

Dachstein Limestone, Monte Canin, Julian Alps, Italy

The Julian Alps are located in the Southern Alps, encompassing northeastern Italy and western Slovenia (Figure 1B). Here, a 700-800 m thick Dachstein Limestone Formation conformably overlies a 1000 m thick sequence of Dolomia Principale Formation, and is succeeded by 50-130 m of Calcari Grigi Formation (Figure 2B). The Dachstein Limestone is subdivided into Lower and Upper members (Ciarapica and Passeri, 1990). The presence of benthic foraminifer *Triasina hantkeni* in the upper member indicates a Late Norian-Rhaetian age (Reijmer and Everaars, 1991; Romano et al., 2008; Gale, 2012); the lower member is probably late Middle Norian in age. There is evidence from the Arabian shelf for *T. hantkeni* significantly below (200 m) the occurrence of a Late Norian ammonoid, *Neotibetities* (Maurer et al., 2008), raising the possibility that a significant portion of the Dachstein in the Julian Alps could reach down into the Middle Norian.

The Lower Member (200-300 m thick) is comprised of m-scale shallowing upward cycles, similar to those of the underlying Dolomia Principale (Bosellini, 1967; Bosellini and Hardie, 1988), with some tepee horizons (Ciarapica and Passeri, 1990). The cycles are characterized by three subfacies (Figure 3): at the base, Subfacies C indicates a subtidal environment, and grades upwards into Subfacies B, homogeneous and laminated "loferites", indicating an inter- to supratidal environment.

The Upper Member (400-500 m thick) lacks tepee zones, but above Subfacies B is an additional Subfacies A with paleosols and evidence of subaerial exposure. Thus, the Lofer cyclothems of the upper member have a definitive, shallowing upward (C-B-A) theme.

A field photograph of Picco di Carnizza at Monte Canin was digitized in grayscale mode (Figure 4A). Three single-pixel vertical scans were taken using the image analysis free software Scion Imageä, and merged into a 224.1-meter-long profile (Figure 4B). This grayscale scan correlates to the lower 60 cycles of a measured section to the southeast at Monte Canin, plus another 60 cycles extending further down in the section (Cozzi et al., 2005). This grayscale proxy reflects facies-dependent weathering: Subfacies C is resistant to weathering, and comprise the vertical surfaces inhospitable to vegetation, resulting in lighter grayscale values. Subfacies A and B are more susceptible to weathering, resulting in recessed zones with vegetation, corresponding to darker grayscale values.

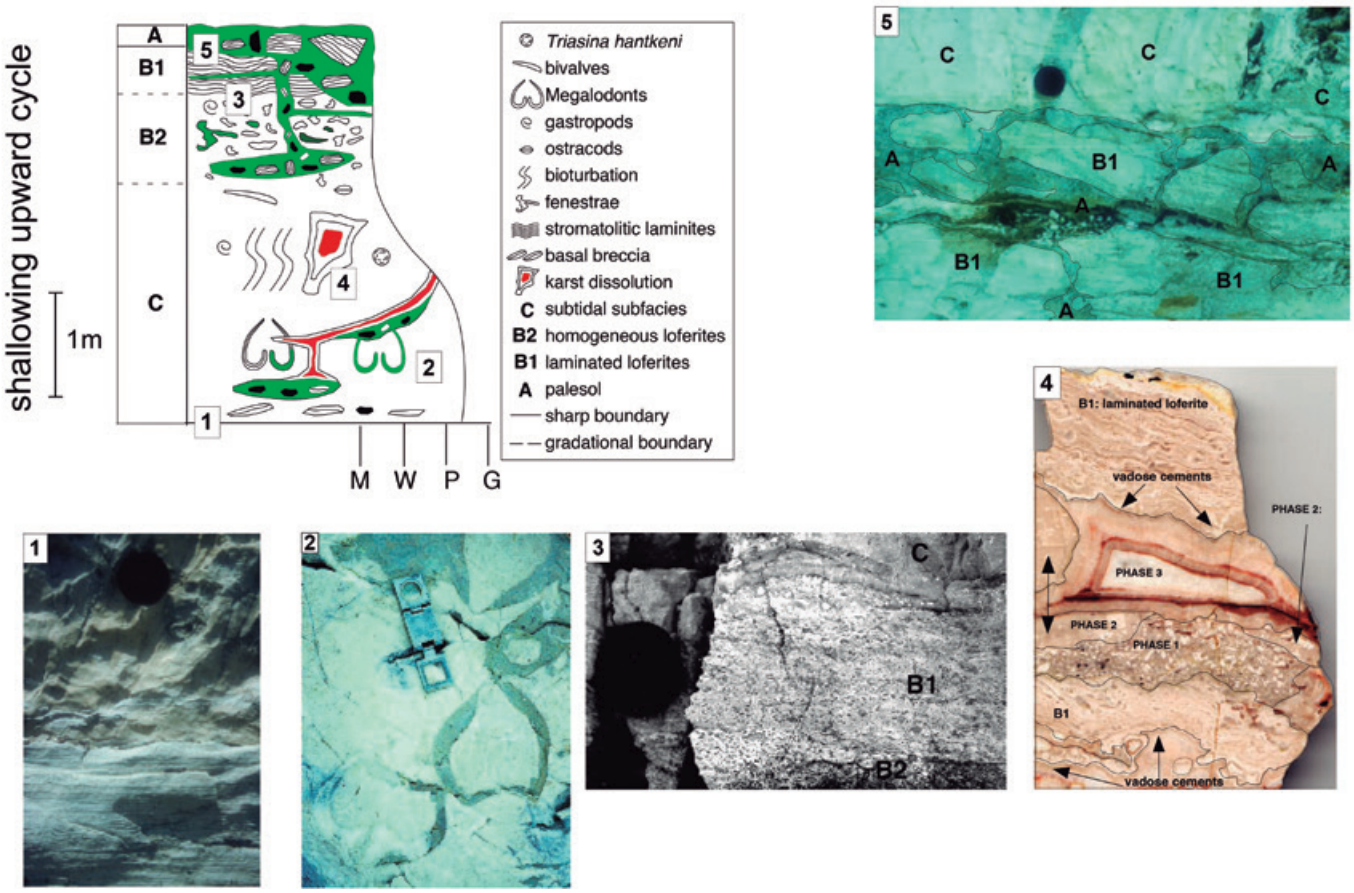

Figure 3. Lofer cyclothem of the Dachstein Limestone (modified from Cozzi et al., 2005). Upper left: Subfacies: A=paleosol, B1=laminated loferites, B2=homogeneous loferites, and C=subtidal megalodont limestone (based on Goldhammer et al., 1990). M=micrite; W=wackestone, P=packstone, and G=grainstone. Photographs: 1. Basal disconformity: erosive basal disconformity between the top of m-scale cycle (B1) and overlying subtidal deposits (C). Flat pebbles eroded from B1 are found at the base of C. Lens cap 5 cm diameter. 2. Megalodont-rich C. The megalodont shells have been partly or totally dissolved and infilled by green marls with cm-size black pebbles of A that percolated down from the top of the cycle. Magnifier is 10 cm long. 3. B1 and B2 sharply overlain by C, with eroded flat pebbles from B1 at the base. 4. Karst features. Phase 1: dissolution and infilling by breccias with blackened clasts and fragments of B1. Phase 2: infilling of karstic dissolution cavity by C with fragments of B1. Phase 3: dissolution and infilling of cavity by marine fibrous and burial cements. 5. Top of cycle disruption by A, with brecciation and partial dissolution of B1, which can occur above and/or below fragments of B1. Lens cap is 5 cm.

Figura 3. *Ciclotema Lofer de la Dachstein Limestone (modificado de Cozzi et al., 2005). Superior izquierda: Subfacies: A=paleosuelo, B1=loferitas laminadas, B2=loferitas homogéneas, y C=calizas subtidales con megalodon (basado en Goldhammer et al., 1990). M=micrita; W=wackestone, P=packstone, y G=grainstone. Fotografías: 1. Disconformidad basal: disconformidad basal erosiva entre la parte superior del ciclo de escala métrica (B1) y los depósitos subtidales suprayacentes (C). Guijarros planos erosionados de B1 se han encontrado en la base de C. La tapa de la lente es de 5 cm de diámetro. 2. C rico en megalodon. Las conchas de megalodon han sido disueltas parcialmente o totalmente y rellenadas por margas verdes con guijarros negros de tamaño centimétrico de A que percolaron hacia abajo desde la parte superior del ciclo. La lupa tiene una longitud de 10 cm. 3. B1 y B2 marcadamente recubierto por C, con guijarros planos erosionados desde B1 en la base. 4. Rasgos kársticos. Fase 1: disolución y relleno por brechas con clastos ennegrecidos y fragmentos de B1. Fase 2: relleno de cavidades de disolución kárstica por C con fragmentos de B1. Fase 3: disolución y relleno de cavidades por cementos marinos. 5. Parte superior del ciclo con disrupción por A, con brechificación y disolución parcial de B1, que puede ocurrir sobre y/o debajo de fragmentos de B1. La tapa de la lente tiene 5 cm.*

Passaic Formation, Martinsville Core, Newark Basin, USA

The subsurface of the eastern margin of North America is characterized by a series of Triassic-Jurassic rift basins that developed during the breakup of the supercontinent Pangea. In New Jersey, these basins are filled with alluvial-fluvial-lacustrine sediments in a more than 5 km-thick, 30 million-year-long sequence that includes the Stockton (alluvial-fluvial), Lockatong (deep to shallow lake), to Passaic (playa lake) formations (Olsen, 1980, 1986, 1990; Smoot, 1991; Smoot and Olsen, 1994; Smoot, 2010). In 1990-1993, the entire sequence was drilled in the Newark Basin (New Jersey, USA) in a series of stratigraphically overlapping, offset drill cores (Kent et al., 1995; Olsen et al., 1996). The Martinsville core (Figure 1C) penetrates the uppermost part of the Passaic Formation through the end of the Triassic Period (Figure 2A). A geomagnetic polarity series was reconstructed for the composite core sequence (Kent et al., 1995), along with a continuously logged facies analysis reported as "depth rank" codes (Olsen, 1986) (Fig-

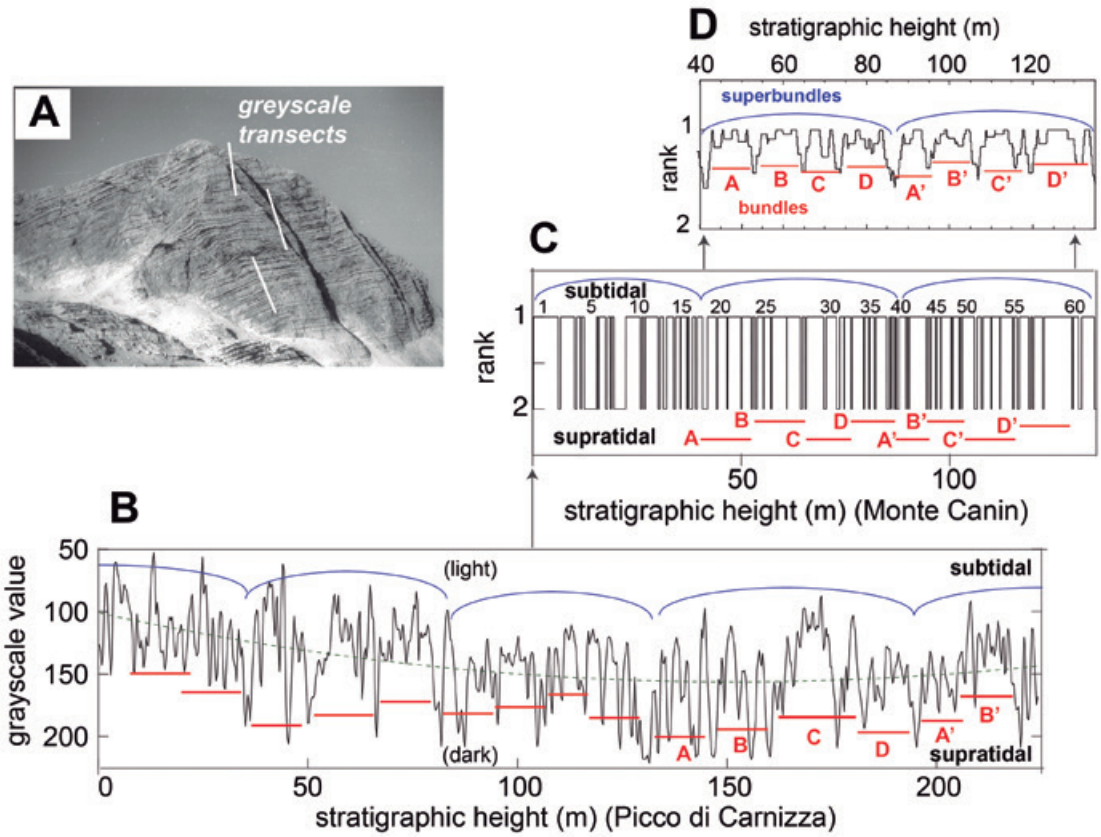

Figure 4. Picco di Carnizza grayscale scan and Monte Canin measured section (part) of the Dachstein Limestone upper member. A. Field photograph of Picco di Carnizza, with scan transects indicated. B. The grayscale scan; the pixel density of the photograph yielded a stratigraphic resolution of 27 pixels per cm, for a total of 224.1 meters. The green dashed curve is a least-squares fitted parabola that is removed prior to spectral analysis. C. Part of the measured section at Monte Canin (Figure 1B) that overlaps the grayscale scan, shown as a subtidal-supratidal rank series. D. A 2-meter smoothed version of C. highlighting the bundles (red) and superbundles (blue) overlapping with B. [Alpine Hippies 10-minute hiking tour: https://www.youtube.com/watch?v=ZEbqX7_nRI0].

Figura 4. *Escaneo en escala de grises de Picco di Carnizza y sección medida (parte) de Monte Canin del miembro superior de la Dachstein Limestone. A. Fotografía de campo de Picco di Carnizza, con indicación de las transversales escaneadas. B. El escaneo en escala de grises; la densidad de pixels de la fotografía da una resolución estratigráfica de 27 píxeles por cm, para un total de 224.1 metros. La curva verde discontinua es la parábola de mínimos cuadrados ajustada y que es sustraída previo al análisis espectral. C. Parte de la sección medida en Monte Canin (Figure 1B) que se sobrepone al escaneo en escala de grises, mostrada como una serie en el rango subtidal-supratidal. D. A version suavizada de C utilizando una ventana de 2 metros, destacando los haces (rojo) y super-haces (azul) que se solapan con con B. [Alpine Hippies 10-minute hiking tour: https://www.youtube.com/watch?v=ZEbqX7_nRI0]*

ure 5), grain size, sediment color, gamma, and sonic velocity, and most recently, XRF core-scanned elements, including iron, calcium and sulfur (Olsen et al., 2019).

The depth rank series of the Martinsville core (Figure 6) indicates that this part of the Passaic Formation is very "dry" – the highest depth rank is between 2 (mudcracked mudstone to heavily burrowed fine sandstone) and 3 (thin-bedded non-mudcracked mudstone), and most depth ranks cycle between 0 (intense breccia or massive rooted/mudcracked mudstone) and 1 (breccia, cement-filled rooted mudstone or fine-rippled sandstone). These facies changes are readily observed along the core, making the depth rank series the best cyclostratigraphic proxy that is currently available for the core.

Methods

The methods applied in this study include astronomical models of Rhaetian Milankovitch cycles, including a newly developed g_2-g_5 astronomical metronome. The cyclostratigraphic proxies are analyzed with standard signal processing algorithms as described below. Both Dachstein and Passaic proxy series are minimally tuned to 405-kyr cycles, and the Passaic series is tied directly to the g_2-g_5 metronome. The Dachstein series additionally undergoes a "tune-and-release" procedure in an attempt to correct for high-frequency sedimentation rates (that do not affect the more depositionally steady Passaic Formation).

Rhaetian Milankovitch cycles

The Milankovitch cycles predict the incoming solar radiation at a specific time and location on the Earth (Milankovitch, 1941). Their accuracy depends on that of the Earth's orbital and rotational parameters. Two factors in the Earth's ancient orbital-rotational parameters are very uncertain: (1) Earth-Moon tidal friction reduces Earth's rotation rate, axial precession and elliptical shape through geologic time, lengthening the periodicities of the obliquity and precession index cycles (Berger and Loutre, 1994); and (2) Solar System chaos involving mainly the inner planets irregularly perturbs the periodicities of the Earth's short (~100 kyr) orbital eccentricity cycles (Laskar et al., 2004, 2011). Despite the uncertainties presented by these factors, Earth's cyclostratigraphy exhibits strong evidence for Milankovitch-forced paleoclimate changes, the premier case in point none other than the Newark Basin record, including the Martinsville Passaic Formation.

Table 2 provides the input rotational parameters used to compute periodicities for three models of Milankovitch cycles in Table 3. Model 0 depicts modern-day Milankovitch cycles according to Laskar et al., (2004). Model 1 back-projects present-day tidal dissipation to estimate precession frequency k at 200 Ma (Laskar et al., 2004). This results in shorter obliquity and precession periodicities, as depicted in Figure 7. Model 2 is based on Waltham (2015), who estimated lunar recession through geologic time constrained by a lunar Roche limit at 4.5 Ga (age of the Moon), and from this constraint, Earth's precession frequency k. Thus, Waltham's k for 200 Ma is significantly lower than Laskar's k; this is reflected in obliquity and precession periodicities that theoretically can be resolved in the data, especially in the longer Passaic series.

The g_2-g_5 metronome

Astronomical solutions of the Earth's long (405 kyr) orbital eccentricity cycle involving the precession of the orbital perihelia of Venus and Jupiter, g_2-g_5, reveal a stable history for the cycle through time, with estimates that diverge less than one 405-kyr cycle over 250-Myr long calculations (Laskar et al., 2004, 2011). A formula based on the La2004 solution of Laskar et al. (2004) for the most recent 405-kyr cycle is provided as a MATLAB script in Hinnov (2018).

New high-precision U-Pb geochronology has validated the phase set by the most recent 405-kyr cycle with respect to the McLaughlin cycles of the Passaic Formation (Kent et al., 2018). The geochronology also rules out the possibility of gaps in the Passaic for the strata younger than 215 Ma, which includes the Rhaetian Martinsville core.

A.

Core Depth (ft)	405-kyr increment
1183.7	0
1414.0	405
1729.0	810
2028.2	1215
2293.5	1620
2616.6	2025
2876.0	2430
3214.5	2835
3503.0	3240
3770.7	3645
4015.0	4050

B.

Stratigraphic height (cm)	405-kyr increment
3510	0
8748	405
13010	810
19520	1215

C.

Stratigraphic height (cm)	100-kyr increment
837	0
2052	100
3510	200
4995	300
6642	400
8181	500
9531	600
10476	700
11610	800
13041	900
14688	1000
16011	1100
17631	1200
19521	1300
20439	1400
22005	1500

Table 4. Stratigraphic definition of cycle boundaries for tuning. **A**. Martinsville Core McLaughlin Cycle definitions (Olsen and Kent, 1996). The average thickness of the McLaughin Cycle is 283 ft. **B**. Picco di Carnizza grayscale scan superbundle boundaries (this study); the mean thickness of the superbundle is 5337 cm. **C**. Picco di Carnizza grayscale scan bundle boundaries (this study); the mean thickness of the bundle is 1411 cm.

Tabla 4. *Definición estratigráfica de límites de ciclo para tuneado. A. Definiciones de Martinsville Core McLaughlin Cycle (Olsen and Kent, 1996). El espesor medio del ciclo McLaughin Cycle es de 283 ft. B. Escaneo de escala de grises de Picco di Carnizza límites de super-haces (este estudio); el espesor medio del super-haz es de 5337 cm. C. Escaneo de escala de grises de Picco di Carnizza límites de haces (este estudio); el espesor medio del haz es de 1411 cm.*

Parameter	La2004	Passaic	Dachstein
Orbital eccentricity	405	436.9*	341*
	130	125.0	-
	97.6	105.7/88.6	108*
Obliquity	34.1	35.4	34.1*
Precession index	21.3	24.5	24.7
	20.1	21.3	19.3
	17.5	17.4	-
	15.3	14.3	15.9

Table 5. Summary of theoretical and observed astronomical periodicities (in kyr). La2004 (**Figure 7**), Passaic depth rank (**Figure 8B**), and Dachstein grayscale (**Figure 9D**). "*" indicates "tuned".

Tabla 5. *Sumario de las periodicidades astronómicas teóricas y observadas (en ka). La2004 (Figure 7), rango de profundidad Passaic (Figura 8B), y escala de grises Dachstein (Figura 9D). "*" indica "tuneado".*

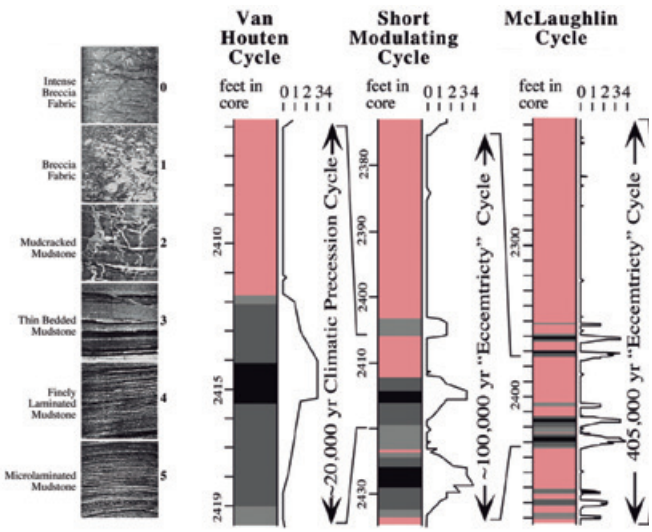

Figure 5. Van Houten, modulating and McLaughlin cycle architecture of the Metlars Member in the Passaic Formation, from Fig. 2 in Olsen et al. (2011). Core photographs are from Fig. 6 in Olsen (2010), illustrating depositional fabrics for depth ranks 0-5. For the Martinsville core, Olsen and Kent (1996, Fig. 4) make note of 'secondary ranks': 0=massive rooted and mudcracked mudstone (1193 ft); 1=cement-filled mudstone (2858 ft); and 'tertiary ranks': 1=fine rippled sandstone (1728 ft) and 2=heavily burrowed fine sandstone (2873 ft).

Figura 5. *Modulación de Van Houten y arquitectura de ciclo de McLaughline del Metlars Member en la Passaic Formation, de Fig. 2 en Olsen et al. (2011). Las fotografías de secciones son de la Fig. 6 en Olsen (2010), ilustrando fábricas deposicionales para rangos de profundidad 0-5. Para la sección Martinsville, Olsen and Kent (1996, Fig. 4) hacen notar 'rangos secundarios': 0=lutita masiva con raices y grietas (1193 ft); 1=lutita rellena de cemento (2858 ft); y 'rangos terciarios': 1=arena con ondulaciones (1728 ft) y 2=arena fina altamente bioturbada (2873 ft).*

Signal processing

The procedures described below were carried out using MATLAB scripts, indicated in *italics* and available in the MATLAB Curve Fitting, Signal Processing, and Statistics and Machine Learning toolboxes; scripts indicated with "*" are by co-author LH may be downloaded from: http://mason.gmu.edu/~lhinnov/cyclostratigraphytools.html

Interpolation

Both Dachstein and Passaic proxy series are equispaced and amenable to methods requiring uniform sampling. However, when tuning is applied, the resulting time scale is non-uniform; linear interpolation is then applied to restore uniform sampling in time, using MATLAB's *interp1.m* function.

Detrending

Detrending was not required for the Passaic series (only subtraction of the mean), but the Dachstein series was processed to remove a parabolic trend through the series using a 2nd order polynomial fit using *polyfit.m* and *polyval.m*. More discussion about this decision appears in Section 4.2 below.

Spectral analysis

Multitaper spectral analysis with 2π prolate tapers (Thomson, 1982) was applied to evaluate average power spectra using *pmtm.m*; unsmoothed FFT spectrograms were computed with *evofft.m** to track changes in frequency content along the proxy series, to identify changes in depositional rate and/or other significant spectral structures. Hypothesis testing is not applied in this study, due to the uncertain timescales which misalign frequency terms that detracts from their apparent significance. This persists even after applying the tuning procedures described in Section 3.4). Methods that estimate spectral backgrounds ("noise") and adopt these as null models rely on high power in the spectrum as the sole criterion for rejecting a null model. This is not an acceptable criterion for astronomical spectra. For example, when obliquity power is low (but present), it will not exceed the spectral background at a statistically significant level. Also, short orbital eccentricity spectral

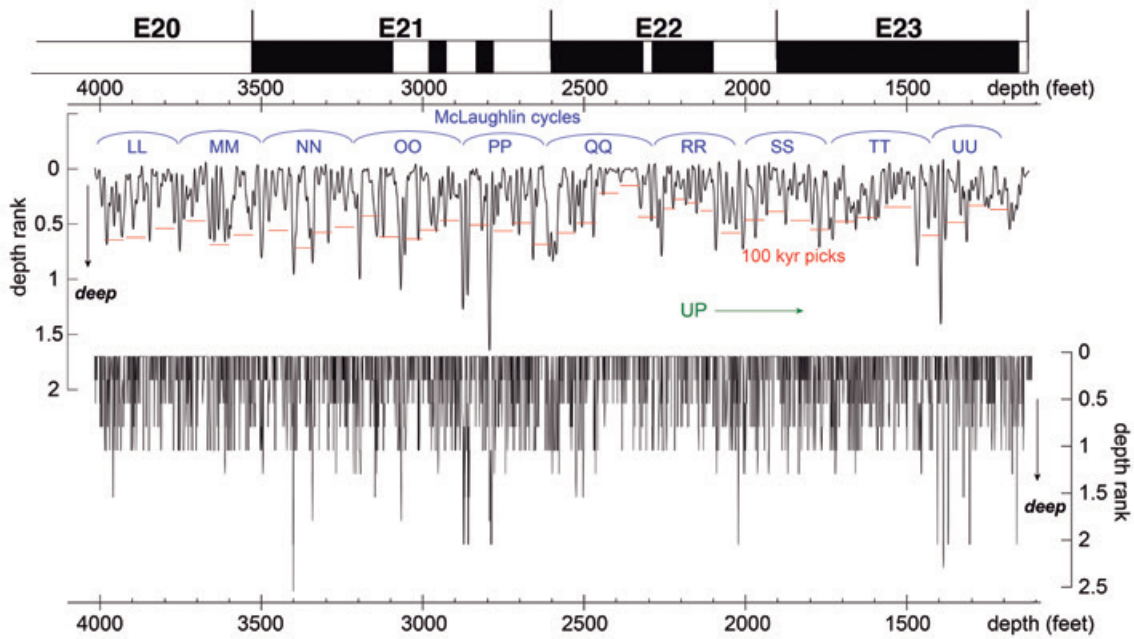

Figure 6. Martinsville Core, depth rank series, 1215.1 ft to 4015.0 ft. A. Smoothed depth rank series, using a 20 ft LOESS fit of the raw depth rank series to emphasize the McLaughlin cycles (blue arcs and text). B. Raw depth rank series. McLaughlin Cycle PP can be compared to Fig. A84 in Smoot (2010), which is from Fig. 18 in Smoot and Olsen (1994).

Figure 6. *Martinsville Core, series de rango de profundidad, 1215.1 ft hasta 4015.0 ft. A. Series de rango de profundidad suavizadas, utilizando un ajuste LOESS de 20 ft de las series originales de rango de profundidad para enfatizar los ciclos de McLaughlin (arcos azules y texto). B. Series originales de rango de profundidad. El ciclo de McLaughlin PP se puede comparer con la Fig. A84 en Smoot (2010), que a su vez es de la Fig. 18 en Smoot and Olsen (1994)*

terms will not register statistically significant levels, either in power spectrum noise hypothesis testing, or in harmonic line testing, even with a perfect timescale (Meyers, 2012). This is because the short orbital eccentricity frequencies perpetually modulate with time, which divides power into multiple spectral terms, none of which are stable long enough to measure at a constant phase. Other issues include sampling rates, and inadvertently including signal when estimating noise background (Hinnov et al., 2016, 2018).

Filtering

LOESS ("locally estimated scatterplot smoothing") estimation, also known as Savitsky-Golay filtering (Savitsky and Golay, 1964), performs least squares regression on a 2nd degree polynomial model in a running window. Here it is applied using *smooth.m* to the Passaic series for better visualization of cyclic patterns. The smoothing function with FFT and shift filter with a 200-cm window in *Analyseries* (Paillard et al., 1996) was used to smooth the Dachstein measured section rank series. The Taner bandpass filter (Taner, 2000) using *tanerfilter.m** was applied to the Dachstein series to isolate a misaligned frequency for minimal tuning (see Section 3.4.2).

Tuning procedures

Tuning of cyclostratigraphy is needed in order to correct for variable sedimentation rates, otherwise cycles will remain misaligned as a function of time and stay hidden. At the same time, tuning can rapidly become an exercise in circular reasoning, and when pursued, interpretations must be adjusted accordingly. Here the principle of "minimal tuning" is described for the Passaic proxy, followed by a "tune-and-release" approach that was additionally attempted on the shorter, more variable Dachstein proxy.

Minimal tuning

One conservative approach is to tune a proxy series to one frequency only, known as "minimal tuning" (Muller and MacDonald, 2000). This allows interpretation of other frequencies in a proxy series relative to the tuned (manipulated) frequency. In fact, tuning to usually prominent 405-kyr cycles in cyclostratigraphic sequences – typically readily observed as superbundles of four ~100 kyr-scale cycles – has become almost "standard procedure", successfully aligning other, higher frequencies related to short orbital eccentrici-

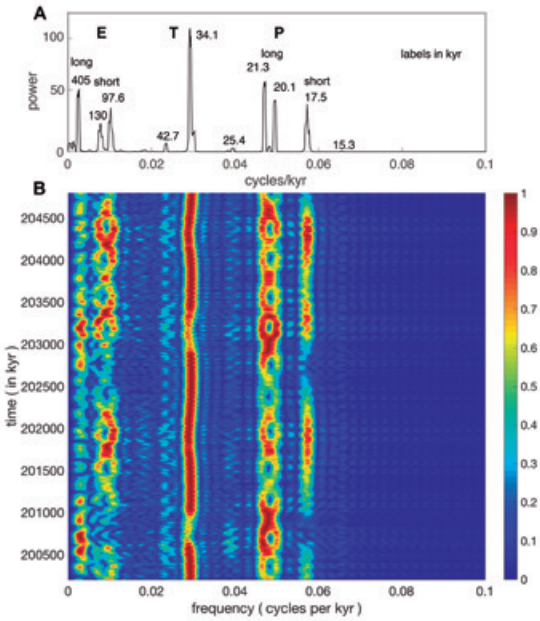

Figure 7. Spectral analysis of ETP series of Rhaetian (200 Ma to 205 Ma) Model 1 astronomical parameters (Tables 2, 3) according to the La2004 solution (Laskar et al. (2004). The ETP series is a synthetic time series comprised of the sum of standardized orbital eccentricity (E), obliquity (T, for "tilt"), and precession index (P) time series from the La2004 solution. (It is shown as a function of time in Figure 10.) Top: 2π multitaper power spectrum; bottom: FFT spectrogram computed with a 400 kyr running window. Note the "braided" pattern of the short orbital eccentricity and long precession index terms.

Figura 7. *Análisis espectral de la series ETP del Rhaetiense (200 Ma a 205 Ma) Modelo 1 parámetros astronómicos (Tablas 2, 3) de acuerdo a la solución La2004 (Laskar et al. (2004). La serie ETP es una serie temporal sintética compuesta por la suma de series temporalis estandarizadas de exentricidad (E), oblicuidad (T, para inclinación), e índice de precesión (P) de la solución La2004. (Se muestra como una función del tiempo en la Figura 10.) Parte superior: 2π multitaper power spectrum; parte inferior: FFT espectrograma calculado con una ventana móvil de 400 ka. Es de notar el patrón "entrelazado" de los términos de los índices de la excentricidad orbital corta y de la precesión larga.*

ty, obliquity and precession index in many cyclostratigraphic sequences (see list in Hinnov, 2018).

Minimal tuning to a "404 ka" cycle of the entire Newark composite series, including the Martinsville core, was undertaken in Olsen and Kent (1999): (1) the composite depth rank series and color series were smoothed using a moving average with a triangular window with a half-length of 27.4 m (=89.9 ft). (2) The two series were zero-phase bandpass-filtered with a low cutoff frequency of 0.00213 cycles/m (=0.000649224 cycles/ft) and a high cutoff frequency of 0.00244 cycles/m (=0.000743712 cycles/ft), designed to isolate the McLaughlin cycles. The smoothed and bandpass-filtered results were averaged together, and are displayed in Fig. 4 of Olsen and Kent (1999) (see also Fig. S10 in Olsen et al., 2019). The maxima of these two curves were taken as tie points and correlated to synthetic 404 ka cycles, which at the time was the estimated periodicity of the g_2-g_5 orbital eccentricity cycle (Laskar, 1999). The Newark series tuned in this way clearly revealed four spectral peaks in the "relative water depth" power spectrum related to the four major terms of the short orbital eccentricity (see Fig. 8 in Olsen and Kent, 1999) (compare with Table 3A).

In the present study, the boundaries of the McLaughlin cycles in the Martinsville depth rank series (Table 4) are assigned times that are multiples of 405 kyr; these times are then substituted by the g_2-g_5 metronome times defined by Laskar et al. (2004) (see Section 3.2). The conversion from depth to time is made on the proxy series using *depthtotime.m**.

Tune-and-release approach

A proxy series may indicate, as in this case the Dachstein proxy, what appear to be 405-kyr cycles, but tuning to them may not successfully align other astronomical frequencies. This may be due to highly variable sedimentation rates that cannot be sufficiently attenuated by 405-kyr tuning only. In such cases, ~100-kyr cycles may be more prominent, and tuning these to 100-kyr intervals may be the best next option. However, for short series, e.g., on the order of 1 million years, with only a few 405-kyr repetitions, due to the wide variability in ~100 kyr orbital eccentricity cycles that can have periods ranging from 90 kyr to 125 kyr to 135 kyr in succession, strict 100 kyr tuning can actually misalign the 405 kyr cycles. Moreover, obliquity and precession index cycles will also experience misalignment. All may appear in spectral analysis as split frequencies at a fraction of their true power. Fortunately, obliquity cycles are relatively monotonic, i.e., with only one major frequency (Figure 7); therefore, misalignment of the obliquity cycle caused by strict 100 kyr tuning can be corrected by "releasing" the 100 kyr tuning, and further tuning the obliquity band to restore its power to a single frequency. This is done by bandpass-filtering the obliquity band of frequencies to isolate the misaligned obliquity cycles, identifying the maxima (using *maxima.m**) and reassigning the times of the maxima to multiples of the obliquity period; in the case of the Rhaetian, this would be 34.1 kyr if tuning to Model 1, or 37 kyr for Model 2 (Table 3). Thus, while the orbital eccentricity and obliquity

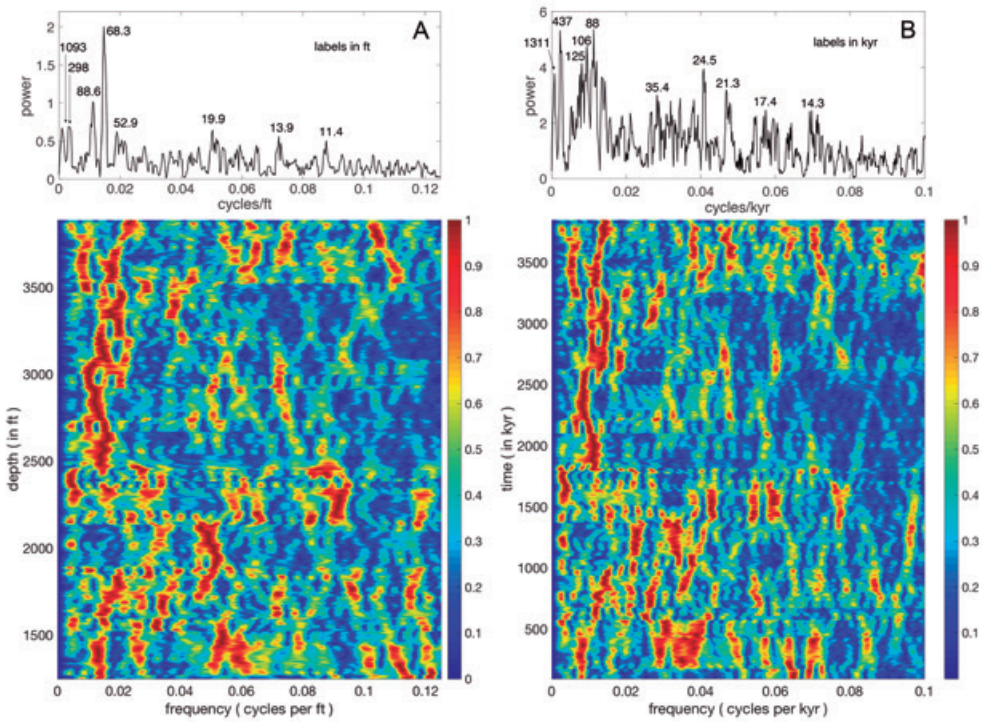

Figure 8. Passaic depth rank spectral analysis. A. Stratigraphic domain: 2π multitaper power spectrum (top); spectrogram with a 250 ft running window (bottom). B. 405-kyr time domain (4159 kyr duration): 2π multitaper power spectrum (top); spectrogram with a 400 kyr running window.

Figura 8. *Análisis spectral del rango de profundidad Passaic. A. Dominio estratigráfico: 2π multitaper power spectrum (parte superior); espectrograma con una ventana móvil de 250 ft (parte inferior). B. Dominio del tiempo de 405-ka (4159 ka de duración): 2π multitaper power spectrum (parte superior); espectrograma con una ventana móvil de 400 ka.*

bands will now have been manipulated by this "tune-and-release" procedure, the precession index band of frequencies can still be interpreted.

Results

The longer Passaic series required the least amount of processing to reveal clear evidence for all three astronomical parameters with only minimal tuning to the 405-kyr cycle. Therefore, the results of the Passaic analysis are presented first. The much shorter Dachstein series proved to be more complicated, requiring a tune-and-release approach to reveal similar evidence. Note: The Martinsville core of the Passaic Formation was curated in depth using "feet" which equals 0.0348 meters.

Passaic Formation

Stratigraphic spectrum

Spectral analysis of the Martinsville raw depth rank series indicates a prevalence of power in the 68.3 ft to 88.6 ft range (Figure 8A); these are the "short modulating cycles" (Figure 5). In the spectrogram, the spectral power has a "braided" pattern that is characteristic of short orbital eccentricity (compare with Figure 7). The clarity of this pattern over the entire lower half of the series suggests that sedimentation rates are relatively steady there; in the top half of the series, the pattern breaks up temporarily and the dominant frequencies shift into the 10 ft to 20 ft range. The McLaughlin cycles (Figure 6) have an average thickness of 283 ft (Table 4), represented by a surprisingly low-power spectral peak at 298 ft; if these cycles represent 405-kyr cycles, then the average sedimentation rate is 0.7 ft/kyr, and the short modulating cycles have periodicities of 97.5 kyr to 126.6 kyr. The Van Houten cycles are represented by low-power spectral peaks at 11.4 ft, 13.9 ft and 19.9 ft, i.e., periodicities of 16.3 kyr, 19.9 kyr and 28.4 kyr, the first two close to the predicted main precession index periods of Model 1 (17 kyr and 20 kyr); the 28.4 kyr cycle is not recognizable.

g_2-g_5 age model spectra

The 405-kyr tuned depth rank series power spectrum (Figure 8B) is in some ways "better" and other ways "worse" than the untuned stratigraphic spectrum

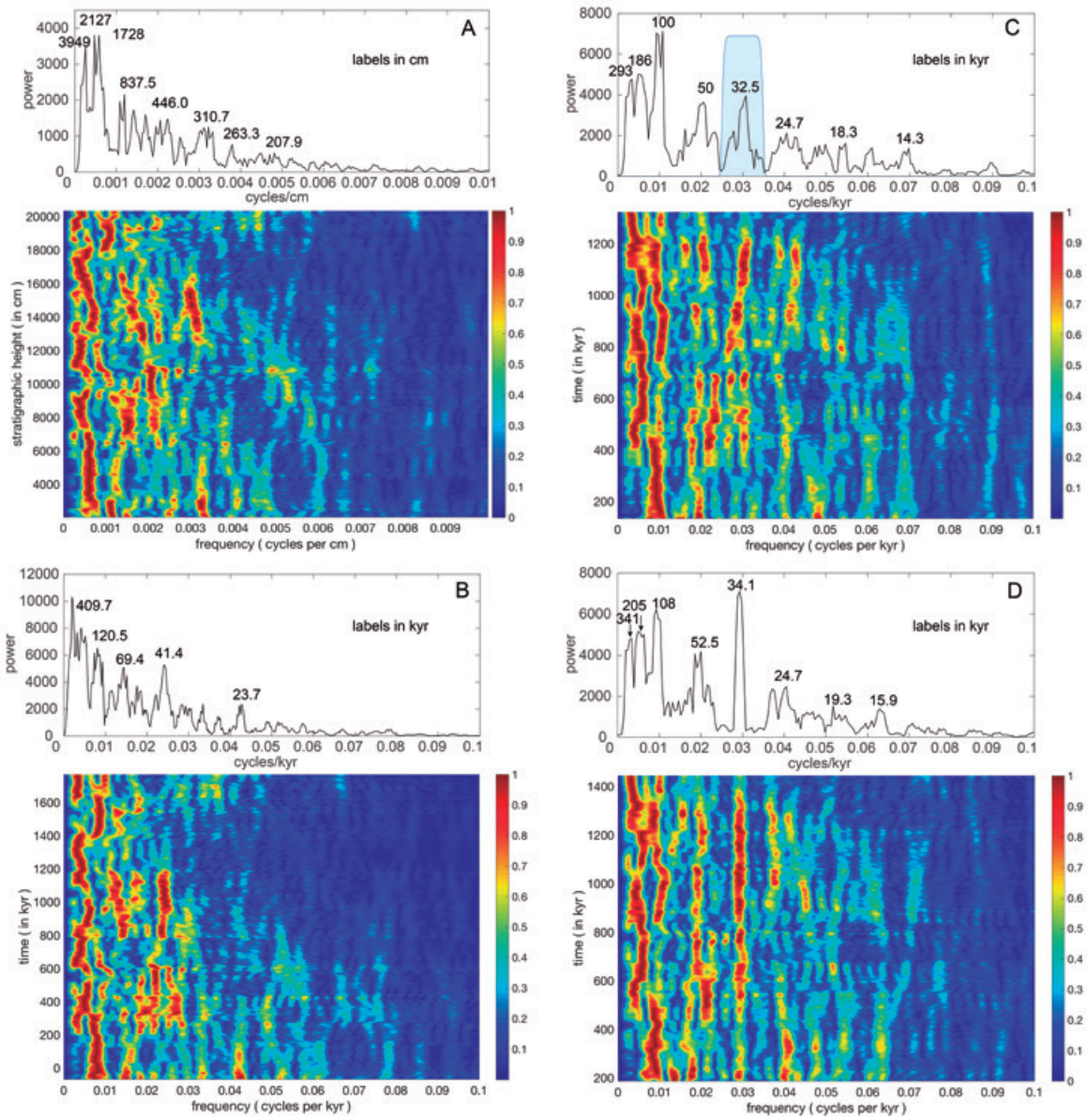

Figure 9. Dachstein grayscale spectral analysis. A. Stratigraphic domain: 2π multitaper power spectrum (top); spectrogram with a 400-cm running window. B. Time domain (2241 kyr duration): 405-kyr tuned 2π multitaper power spectrum (top); spectrogram with a 400-kyr running window. C. Time domain (1592 kyr duration): 100-kyr tuned 2π multitaper power spectrum (top); spectrogram with a 400-kyr running window. D. Time domain (1661 kyr duration): 34.1-kyr tuned 2π multitaper power spectrum (top); spectrogram with a 400-kyr running window.

Figura 9. *Análisis spectral de la escala de grises de Dachstein. A. Dominio estratigráfico: 2π multitaper power spectrum (parte superior); espectrograma con una ventana móvil de 400-cm. B. Dominio del tiempo (duración 2241 ka): 2π multitaper power spectrum tuneado a 405-ka (parte superior); espectrograma con una ventana móvil de 400-ka. C. Dominio del tiempo (duración 1592 ka): 2π multitaper power spectrum (top) tuneado a 100-ka; espectrograma con una ventana móvil de 400-ka. D. Dominio del tiempo (duración 1661 ka): 2π multitaper power spectrum tuneado a 34.1 ka (parte superior); espectrograma con una ventana móvil de 400-ka.*

(Figure 8A). High spectral power clusters at periodicities in the short orbital eccentricity band (125 kyr, 105.7 kyr, and 88.6 kyr), obliquity band (35.4 kyr), and precession index band (21.3 kyr and 17.4 kyr), and the peak at 14.3 kyr may represent the small predicted 15.3 kyr term (see Table 4.2 in Hinnov and Hilgen, 2012). On the other hand, the tuned spectrum is much "noisier" (i.e., variable) than the untuned spectrum, short orbital eccentricity power is not concentrated into two narrow bands (compare with Figure 7), and a high-power peak occurs at 25.4 kyr that is not recognizable.

Dachstein Limestone

Stratigraphic spectrum

The Dachstein untuned grayscale scan replicates, with some differences related to processing parameters, the results of Fig. 3 in Cozzi et al. (2005) (Figure 9A). Notably, this spectrum is almost identical to that of the Dachstein Lofer section displayed in Fig. 8.3 of Schwarzacher (1993), in which the 17.13 m cycle was identified as the "R" cycle and the 2.6 m cycles within R cycles as "r" cycles, well-known from earlier field studies (Schwarzacher 1947, 1954). Another similar spectrum from the Trans-Danubian (Hungarian) borehole PO-89 is displayed in Fig. 8.6 of Schwarzacher (1993).

In the Dachstein spectrum, there is an exponential decline in power from low to high frequency that could be interpreted as evidence for a red noise process (compare with Fig. 1F in Meyers, 2012). However, the 5:1 to 6:1 bundling (Schwarzacher's r cycle) and 4:1 superbundling (Schwarzacher's R cycle) in the measured section (Figures 4B-D) strongly hints that the superbundling is evidence for the g_2-g_5 405-kyr cycle.

The average thickness of the superbundle cycle is 5337 cm, and cannot be clearly resolved in the 2p multitaper power spectrum, which averages over 3 Rayleigh spacings, i.e., 3/22410 cm = 0.0001339 cycles/cm (that is, the 1/5337 cm=0.0001874 cycles/cm frequency is measured incompletely between the first and second frequency bins in this spectrum). Complicating the situation is a parabolic trend affecting the grayscale series (Figure 4B), which appears in the spectrum at f=0 with high power that exceeds all other parts of the spectrum and leaks into the adjacent frequencies. Therefore, this parabola was estimated and removed prior to the spectral analysis.

Tune-and-release age model spectra

The first step taken was to tune to the superbundles as 405 kyr cycles (Table 4B; Figure 9B). This resulted in a slightly less variable spectrum, with spectral peaks at 120.5 kyr and 69.4 kyr, and notably an elevated peak at 41.4 kyr near the obliquity band range, and a well-defined but low-power spectral peak at 23.7 kyr. However, the spectrogram indicates that cycle frequencies along the series are still quite variable, suggesting that high-frequency sedimentation rates not corrected by the 405-kyr tuning still affect the timescale. To test this idea, the bundles were tuned instead to multiples of 100 kyr (Table 4C; Figure 9C). This had the effect of moving all of the spectral peaks to higher frequencies, sharpening the peak centered on the 32.5 kyr period, and elevating power in the precession index band. In the spectrogram, the 32.5 kyr term drifts and is split in some intervals, and so a final tuning was attempted to straighten this term and assign it a single period of 34.1 kyr (the Model 1 main obliquity period, see Figure 7). This was accomplished by bandpass-filtering the 32.5 kyr term in the 100-kyr tuned series, and assigning successive maxima of the filtered signal to multiples of 34.1 kyr (Figure 9D).

The obliquity tuning successfully (albeit artificially) gathered substantial power into a single term at 34.1 kyr, while also linearizing almost all of the signal components in the precession index band. There is a 50 kyr term that continues through nearly the entire spectrogram; with every tuning step, it sharpens and straightens. There is also a curious term at 24.7 kyr that also sharpens and strengthens with each tuning step; it is reminiscent of the sharp 24.5 kyr term in the 405-kyr tuned Passaic spectrum (Figure 8B).

Discussion

The evidence for Rhaetian Milankovitch cycles

Of the two proxies, the longer (4159 kyr estimated duration) Passaic depth rank series shows the most (and best) evidence for astronomical forcing: tuning with the McLaughlin cycles and accepting that they represent g_2-g_5 405-kyr cycles readily aligned the majority of variations into clearly discernible astronomical terms (Figure 8B, Table 5). Below is an explanation of how the McLaughlin cycles have come to be assigned to specific g_2-g_5 metronome times and supported by radioisotope geochronology (Section 5.3). There is a preponderance of power in the ~100 kyr band; in fact, in the original stratigraphic spectrum (Figure 8A), power is confined to two narrow bands centered on 126.6 kyr (88.6 ft) and 97.5 kyr (68.3 ft). Of some surprise is the existence of a not very weak obliquity term at 35.4 kyr, especially toward the top of the series. This is a rare appearance of obliquity in a tropical paleoclimate series that is well known for the absence of obliquity forcing (e.g., Olsen et al., 2019). Multiple precession index band terms are detected (21.3 kyr, 17.4 kyr and 14.3 kyr) although they do not display a "braiding" pattern in the spectrogram (compare with the precession index in Figure 7). The 24.7 kyr term is not predicted by the La2004 solution, but a similar term is persistent in the extended Newark series (e.g., Fig. 16 in Olsen and Kent, 1996, where power in the long precession band is distributed broadly toward lower frequencies).

The significantly shorter (1661 kyr estimated 34.1 kyr tuned duration) Dachstein grayscale series suffers in comparison: 405-kyr minimal tuning does not

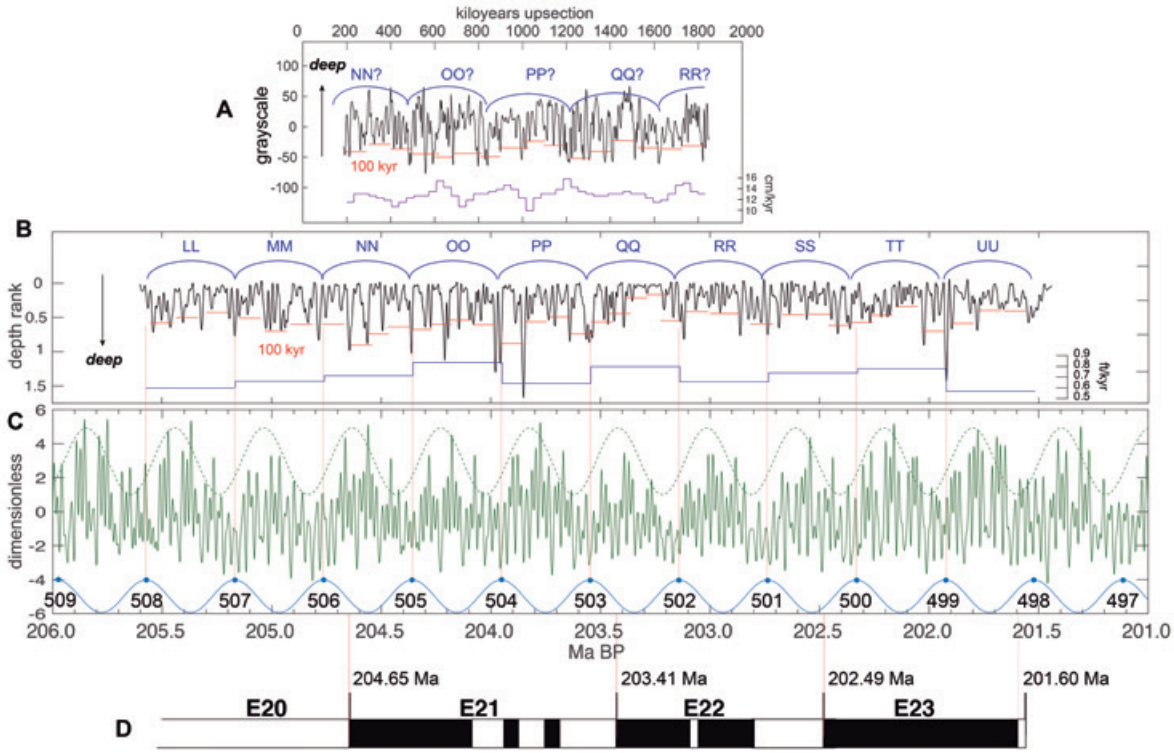

Figure 10. Tentative Dachstein-Newark correlation. A. Tuned Dachstein grayscale series, parabola removed. Superbundles (blue arcs) are labeled with McLaughlin cycle designations with question marks; bundles of 5 to 6 Lofer cyclothems are indicated by red horizontal lines. Light grayscale values indicate deeper subtidal facies (pointing upward). Sedimentation rates (purple) are from the final 34.1 kyr tuning, with an average rate of 22410 cm / 1661 kyr = 13.5 cm/kyr. B. Tuned Martinsville Passaic LOESS-smoothed depth rank series, with McLaughlin cycles now each 405-kyr long (blue arcs and blue text); within them are ~100 kyr cycles (red horizontal lines). Shallow-exposure depth ranks (0 and 1) point upward. Sedimentation rates (blue horizontal lines) are based on the 405-kyr tuning; the average rate for the entire series is 0.700 ft/kyr. C. The La2004 astronomical solution (Laskar et al., 2004) displayed as an ETP series (green); the 405-kyr cycle extracted from the ETP series is shown in dashed green. The g_2-g_5 metronome cycles are shown in aqua and numbered according to their ordination from the most recent 405-kyr cycle (which is g_2-g_5 Cycle No. 1). The aqua dots show the start times for each g_2-g_5 cycle, and their coincidence with the boundaries of the McLaughlin cycles (vertical thin red lines). D. The magnetic reversals measured on the Martinsville Core, and their assigned times with respect to the g_2-g_5 metronome.

Figura 10. *Tentativa de correlación Dachstein-Newark. A. Series tuneadas se escalas de grises Dachstein, con una tendencia parabólica sustraida. Los super-haces (arcos azules) están etiquetados con designaciones del ciclo McLaughlin cycle con signos de interrogación; haces de 5 a 6 ciclotemas Lofer están indicados con líneas horizontales rojas. Valores claros de la escala de grises indican facies subtidales más profundas (apuntando hacia arriba). Los ratios de sedimentación (morado) son del tuneado final a 34.1 ka, con un ratio medio de 22410 cm / 1661 ka = 13.5 cm/ka. B. Series, con suavizado LOESS, de rangos de profundidad tuneadas Martinsville Passaic, con ciclos McLaughlin de 405-ka de duración (arcos azules y texto azul); dentro de los cuales hay ciclos de ~100 ka (líneas rojas horizontales). Los rangos de profundidad de exposición somera (0 y 1) apuntan hacia arriba. Los ratios de sedimentación (líneas azules horizontales) están basadas en el tuneado de 405-ka; el ratio medio para la serie entera es de 0.700 ft/ka. C. La solución astronómica La2004 (Laskar et al., 2004) mostrada como una serie ETP (verde); el ciclo de 405-kyr extraido de la serie ETP se muesra en discontínuo y color verde. Los ciclos de metrónomo g_2-g_5 se muestran en aqua y numerados de acuerdo a su ordenación desde el ciclo de 405-ka más reciente (el cual es el Ciclo g_2-g_5 No. 1). Los puntos aqua muestran el comienzo de las series para cada ciclo g_2-g_5, y su conincidencia con los límites de los ciclos de McLaughlin cycles (líneas delgadas verticales de color rojo). D. Las inversiones magnéticas medidas en el Martinsville Core, y sus tiempos asignados con respecto al metrónomo g_2-g_5.*

readily align other astronomical frequencies, but the tune-and-release approach reduces spectral variability while sharpening precession index band terms at 19.3 kyr and 15.9 kyr, somewhat shorter than La2004 solution periodicities (21.3 kyr, 20.1 kyr and 17.5 kyr), and "braiding" of the terms is not evident in the spectrogram (Figure 9D). The final obliquity tuning also sharpens a term at 24.7 kyr, which is not predicted by the La2004 solution, but it also occurs in the Passaic series (see above). In summary, the evidence for Milankovitch cycles in the Dachstein based on this study is marginally better than for previous analyses, but much improvement is still possible and desirable (see Section 5.5).

Implications for Earth's tidal dissipation history

Two models for tidal dissipation are considered in this study: Model 1 extrapolates present-day rates back to 200 Ma (Laskar et al., 2004), but if extended further back in time, predicts that the Moon's Roche Limit (the point at which the Moon breaks up and crashes

into the Earth) will be reached at 1.5 Ga (e.g., Bills and Ray, 1999). Model 2 instead constrains tidal dissipation so that the Moon's Roche Limit occurs at the age of the Moon (4.5 Ga). The difference between the two models should be distinguishable at 200 Ma, where, for example, Model 1 indicates a main obliquity periodicity of 34.308 kyr to 33.342 kyr, and Model 2 indicates 37.107 kyr to 35.979 kyr (Table 3). The minimally processed Passaic series indicates a term at 35.4 kyr (Figure 8B), which is squarely between the Model 1 and 2 estimates. The tuned Passaic precession index terms (not counting the puzzling term at 24.7 kyr), 21.3 kyr and 17.4 yr, are closer to the Model 1 terms (21.287 kyr, 20.226 kyr, 17.515 kyr and 17.386 kyr) than to the Model 2 terms (22.332 kyr, 21.167 kyr, 18.217 kyr and 18.077 kyr). It should be emphasized that there are many unknowns at issue concerning actual k and g_i at 200 Ma, and advanced modeling is required (e.g., optimization as in Meyers and Malinverno, 2018). However, it is comforting that both the Passaic and Dachstein proxies point to credible values for tidal dissipation between present-day values and the interpolated value at 200 Ma between today and 4.5 Ga.

The g_2-g_5 metronome and a provisional Dachstein-Newark correlation

According to Table 2 in Kent et al. (2017), the top of the Pine Ridge McLaughlin cycle (base of Exeter Township McLaughlin cycle) has an age of 201.60 Ma (near start of g_2-g_5 cycle no. 498). The base of the Pine Ridge McLaughlin Cycle is assigned to g_2-g_5 Cycle 499 (201.91 Ma); and the base of each of the other McLaughlin cycles in downward succession is assigned the next older g_2-g_5 cycle (Figure 10). This "astronomical time scale", defined by the present-day g_2-g_5 orbital eccentricity model, has been shown to be phase-locked with radioisotope geochronology tied to specific Newark magnetozones and g_2-g_5 metronome-calibrated McLaughlin cycles (e.g., E16r and g_2-g_5 Cycle 519) (Kent et al., 2018). It should be emphasized that the g_2-g_5 metronome is different from the 405 kyr cycle in the 200 Ma to 206 Ma La2004 solution (compare dashed green and blue curves in Figure 10C). If this is confirmed with more geological evidence, then the g_2-g_5 model can be better constrained, which will improve the overall astronomical solution.

The Dachstein grayscale scan ostensibly fits somewhere within the Passaic depth rank series, the latter representing the Rhaetian Stage in its entirety. With its sequence of four superbundles, there are a limited number of possible correlations. Additionally, it seems reasonable to assume that when sea level was high leading to Dachstein subtidal units (light grayscale values) it was conversely relatively dry on land leading to shallow to exposure playa facies in the Passaic Formation (low depth ranks). The grayscale scan positioned this way has a profile that compares particularly closely with the depth rank profile through the Passaic OO and PP McLaughlin Cycles. Thus, a provisional link can be established between the two formations (Figure 10A, B).

Marine-continental aquifer-limno-eustasy

The repeating Subfacies C-Subfacies B-Subfacies A succession of the Lofer cyclothems record a history of relative sea level oscillations. Karstic features reaching down as much as 10 meters below Subfacies A suggest that sea level dropped significantly below the platform top during exposure times (Fischer 1964). The question has arisen of whether these sea level oscillations were allocyclic eustatic responses or autocyclic responses to processes operating within carbonate platforms (e.g., progradation) (Ginsburg, 1971; Goldhammer et al., 1990; Satterley and Brandner, 1995; Satterley, 1996a,b). It is reasonable to conclude that both allocyclic and autocyclic forcing played a role, interacting with feedbacks in generating peritidal carbonate cyclicity (Dunn, 1991; Goldhammer et al., 1993; Bazykin, 1998; Demicco, 1998). While the relative roles played by these two forces is open to debate, given the similarities especially between the Dachstein superbundles and Passaic McLaughlin cycles, it is difficult not conclude that Milankovitch-forced sea levels had something to do with generating the Lofer cyclothems, at least at Monte Canin. It is plausible that when sea level oscillations had higher amplitudes across the Dachstein Platform, resulting in thicker subtidal units, there was less water on Laurentia, and the playa lake deposits of the Passaic Formation became more intensely dessicated (Figure 10).

A dynamic land-sea water balance forced by Milankovitch cycles is easily understood when the land reservoir is a cryosphere, but is far less well understood when there is no cryosphere, for example during hothouses, including the Late Triassic Period. The evidence for high-frequency sea level oscillations during non-glacial times keeps growing, and requires an alternative explanation. This has given rise to the concepts of limno-eustasy and aquifer-eustasy that consider the role of variable land water storage in lakes and groundwater in marine eustasy. Estimates of present-day capacity of aquifers in the upper 1 km of the continents is equivalent to ±50 m; this is believed to be a minimum estimate (due to present-day

ice age) and ancient hothouses may have involved much higher (double) volumes (Hay and Leslie, 1990). Jacobs and Sahagian, (1993, 1995) carried the argument further by specifically considering the Late Triassic Newark-Dachstein example, and the Milankovitch forcing of specific latitudes on land to produce, for example, precession-dominated signals in the depositional record. Balog et al. (1997) relied in part on these concepts to argue for an eustatic origin of the Lofer cyclothems. Aquifer-limno-eustasy continues to grow as a viable alternative explanation for high-frequency sea level oscillations during hothouses (Wagreich et al., 2014; Wendler et al., 2016; Haq, 2018; Li et al., 2018).

Future research lines

The provisional Dachstein-Passaic correlation proposed here (Figure 10) needs verification, which must take place with further data collection and analysis, as follows.

Chemostratigraphy

A detailed marine carbonate isotope stratigraphy for the Rhaetian Stage has been underway for decades to understand the timings and effects of the Central Atlantic Magmatic Province eruptions on the carbon cycle and climate (review in Zaffini et al., 2018). Carbonate carbon isotopes at Monte Canin along the measured section (Figure 2l), and elsewhere, e.g., drill cores in Hungary (Balog et al., 1997) can be collected to develop correlations to the global Rhaetian carbon isotope stratigraphy, with a focus on excursions as potential tie points.

Magnetostratigraphy

The Rhaetian Passaic Formation of the Martinsville Core yielded a high-quality sequence of magnetic reversals (Kent et al., 1995) that has yet to be unambiguously correlated to marine magnetostratigraphy (Muttoni et al., 2010; Kent et al., 2017). Marton and Haas (1996) investigated paleomagnetism of Lofer cyclothems in the Transdanubian Range (Gerecse Mountains, Hungary), and determined signal preservation was best in Subfacies A, with positive susceptibility and relatively strong natural remanence magnetism. Both positive and negative polarities were observed in Subfacies A in short (2-5 m) sections at Labatlan Quarry. Reconnaissance studies could be carried out along the measured section (Figure 2l) at the expansive Monte Canin section, where tectonics has had a relatively low influence with a lower likelihood of remagnetization.

New cyclostratigraphic proxies

Lessons learned from the platform carbonates of the Lower Cretaceous Cupido Formation (Hinnov et al., 2013) suggest that high-quality, high-resolution, non-destructive rock magnetic series could be obtained from the Dachstein Limestone, and especially from the Monte Canin section. For example, an anhysteretic remanent magnetism series could be developed to track eolian dust flux into the Dachstein.

Other Rhaetian marine formations with global chronostratigraphic attributes should also be explored, e.g., the Kössen Formation, which has an ammonite zonation and exhibits Milankovitch-scale cyclicity (Mette et al., 2016).

For the Passaic Formation, XRF core-scanned elemental series, e.g., Ca, S and Fe (Olsen et al., 2019) would provide ultra-high-resolution proxies tracking dessication intensity vs. detrital influx into the Rhaetian Passaic playa. Cyclostratigraphy from other continental Rhaetian deposits, e.g., the Chinle Formation of the western USA, is the focus of an ongoing International Continental Drilling Program project in Colorado (Olsen et al., 2018).

Improved signal correlation techniques

New tools for cyclostratigraphic analysis and correlation have recently been made available as freeware, notably Astrochron (Meyers, 2014), which includes advanced modeling with optimization techniques, and Acycle (Li et al., 2019), an alternative to Astrochron, with many equivalent functions but not the advanced modeling, e.g., Astrochron's unique TimeOptMCMC function. These tools have eased the processing burdens required for cyclostratigraphy, but in the process, have identified a new need: interactive signal correlation. There are sophisticated statistical correlation methods available that are customized for cyclostratigraphy, notably Match (Lisiecki and Lisiecki, 2002) and HMM-Match (Lin et al., 2014), and most recently, dynamic time warping (e.g., MyDTW; Kotov and Pälike, 2017).

Conclusions

This study sought evidence for Milankovitch cycles in the Rhaetian marine Dachstein Lofer cyclothems, Julian Alps, Italy, and in the coeval continental Passaic Formation of the Newark Basin (Martinsville Core), New Jersey, USA. The results are summarized as follows.

- The Dachstein Limestone was represented by a grayscale proxy series of its subtidal-supratidal

carbonate cycles at Monte Canin (Picco di Carniza), in which 5-6 Lofer cyclothems per bundle, and 4 bundles per superbundle were readily detected. Only part of the Rhaetian Stage is represented. The superbundles were assumed to represent 405-kyr orbital eccentricity cycles, and the bundles ~100 kyr orbital eccentricity cycles. Minimal tuning to 405-kyr intervals did not successfully align the other astronomical frequencies, presumably due to pervasively varying sedimentation rates along the proxy series. A tune-and-release approach was undertaken, first tuning to 100 kyr intervals, then to 34.1 kyr intervals; the results aligned the two main precession index terms.

- The Passaic Formation was represented by a depth rank proxy series of shallow to exposure facies of a playa lake. The proxy series is characterized by McLaughlin cycles that were originally (sedimentologically) defined along the formation, and that recently were found to be phase-locked with the g_2-g_5 (405-kyr) metronome defined by the La2004 astronomical solution. Minimal tuning the McLaughlin cycles to 405-kyr intervals successfully aligned short orbital eccentricity, obliquity and precession index terms; no further tuning was necessary. The 405-kyr tuned Passaic proxy series indicates a 4159 kyr duration for the Rhaetian stage, in excellent agreement with radioisotope geochronology indicating 4.14±0.39 Myr.
- The estimated frequencies of the obliquity and precession index terms of both proxy series fall between those of the La2004 astronomical solution and Waltham Milankovitch calculator. The obliquity power in the spectra of both proxy series is much stronger than originally supposed. Both proxy series share a 24.7 kyr term that is not predicted by the astronomical solutions.
- The 405-kyr cycles in both proxy series allows for a provisional correlation between the Dachstein and Passaic formations, assuming that the Dachstein subtidal facies (more water in ocean) correlates to Passaic exposure facies (less water on land) as would be consistent with limno-aquifer eustasy.

Acknowledgments

The study presented here was inspired by the Alpine carbonate sedimentology giants of yore, Bruno Sander, Walther Schwarzacher and Alfred Fischer. Bruno Sander's extensive research on "Rhythmically deposited Triassic limestones and dolostones" (Sander, 1936, 1951) continued to advance into the 21st century along two brilliant research lines: (1) Walther's quantitative evaluation of carbonate rhythmic deposition, and (2) Al's qualitative evaluation of carbonate depositional environments. Their peers were deeply appreciative of their collective body of work, which in turn inspired the next generation of researchers, including both of us, LH and AC, to pursue the groundbreaking ideas elucidated by these three giants. We especially thank Walther for his enormously influential books: *Sedimentation Models and Quantitative Stratigraphy* (1975), and *Cyclostratigraphy and the Milankovitch Theory* (1993). And despite our efforts here, as discussed in Section 5.5, much has yet to be accomplished to unravel the mysteries of the Lofer cyclothems.

References

Balog A., Haas J., Read J.F. and Coruh, C., 1997. Shallow marine record of orbitally forced cyclicity in a Late Triassic carbonate platform, Hungary. *Journal of Sedimentary Petrology*, 67, 661-675.

Bazykin, D.A., 1998. *The origin of depositional cycles in shallow marine carbonates: an approach using coupled computer modeling and time series analysis*, Ph.D. dissertation, The Johns Hopkins University, Baltimore, MD, 374 p.

Berger, A., and Loutre, M.-F., 1994. Astronomical forcing through geologic time. In: DeBoer, P.L., Smith, D.G. (Eds.), Orbital Forcing and Cyclic Sequences: *International Association of Sedimentologists Special Publication*, 19, 15-24.

Bills, B.G. and Ray, R.D. 1999. Lunar orbital evolution: a synthesis of recent results. *Geophysical Research Letters*, 26(19), 3045-3048.

Blackburn, T.J., Olsen, P.E., Bowring, S.A., McLean, N.M., Kent, D.V., Puffer, J., McHone, G., Rasbury, E.T., and Et-Touhami, M., 2013, Zircon U-Pb geochronology links the end-Triassic extinction with the Central Atlantic Magmatic Province. *Science*, 340, 941-945.

Ciarapica G. and Passeri L., 1990. The Dachstein Limestone of the Mt. Canin (Julian Alps) and its paleogeographic meaning. *Italian Journal of Geosciences*, 109, 239-247.

Cozzi, A., Hinnov, L.A., and Hardie, L.A., 2005. Orbitally forced Lofer cycles in the Dachstein Limestone of the Julian Alps (NE Italy), *Geology*, 33, 789-792.

Demicco, R.V., 1998. CYCOPATH-2D – A two-dimensional, forward model of cyclic sedimentation on carbonate platforms, *Computers and Geosciences*, 24(5), 405-423.

D'Argenio, B., Horváth, F. and Channell, J.E.T., 1980. Palaeotectonic evolution of Adria, the African promontory. In: Geologie des chaines alpines issues de la Tethys, Aubouin, J., Debelmas, J. and Latreille, M. (eds.), *Mémoires du Bureau de Recherches Géologiques et Minières*,115, 331-351.

Dunn, P.A., 1991. *Diagenesis and cyclostratigraphy: an example from the Middle Triassic Latemar platform, Dolomite Mountains, northern Italy*. Ph.D. dissertation, The Johns Hopkins University, Baltimore, Maryland, 567 p.

Egenhoff, S.O., Peterhänsel, A., Bechstädt, T., Zühlke, R. and Grötsch, J., 1999. Facies architecture of an isolated carbonate platform: tracing the cycles of the Latemàr (Middle Triassic, northern Italy. *Sedimentology*, 46, 893-912.

Enos P.L. and Samankassou E., 1998. Lofer Cyclothems Revisited (Late Triassic, Northern Alps, Austria). *Facies*, 38, 207-228.

Fischer A.G., 1964. The Lofer Cyclothems of the Alpine Triassic. In: Merriam, D.F. (ed.), Symposium on Cyclic Sedimentation. *Kansas Geological Survey Bulletin*, 169, 107-149.

Flügel E., 2002. Triassic reef patterns. In: Kiessling W., Flügel E., and Golonka J. (eds.), Phanerozoic Reef Patterns. *Society for Sedimentary Geology, Special Publication*, 72, 391-463.

Forkner, R.M., 2007. *Depositional periodicity and the hierarchy of stratigraphic forcing in the Triassic carbonates of the Dolomite Alps*, N. Italy. Unpublished Ph.D. Dissertation, University of Texas at Austin, Austin TX, 440 p., 1 Plate.

Gale, L., 2012. Rhaetian foraminiferal assemblage from the Dachstein Limestone of Mt. Begunjščica (Košuta Unit, eastern Southern Alps), *Geolija,* 55(1), 17-44.

Ginsburg, R.N., 1971. Landward movement of carbonate mud: new model for regressive cycles in carbonates, abstract, *American Association of Petroleum Geologists Bulletin*, 55, 340.

Goldhammer, R.K., Lehmann, P.J., and Dunn, P.A., 1993. The origin of high-frequency platform carbonate cycles and third-order sequences (Lower Ordovician El Paso Gp, West Texas): constraints from outcrop data and stratigraphic modeling. *Journal of Sedimentary Petrology,* 63(3), 318-359.

Goldhammer R.K., Dunn P.A. and Hardie L.A., 1990. Depositional cycles, composite sea-level changes, cycle stacking patterns, and the hierarchy of stratigraphic forcing: examples from Alpine Triassic platform carbonates. *Geological Society of America Bulletin*, 102, 535-562.

Goldhammer, R.K., Dunn, P.A., and Hardie, L.A., 1987. High-frequency glacio-eustatic sea level oscillations with Milankovitch characteristics recorded in Middle Triassic platform carbonates in Northern Italy. *American Journal of Science*, 287, 853-892.

Gradstein, F.M., Ogg, J.G., Schmitz, M.D, and Ogg, G.M., 2012. *The Geologic Time Scale 2012*, Elsevier, Amsterdam, 1144 p.

Haas, J., 1982. Facies analysis of the cyclic Dachstein Limestone Formation (Upper Triassic) in the Bakony Mountains, Hungary. *Facies*, 6(1), 75-83.

Haas J., 1994. Lofer cycles of the Upper Triassic Dachstein platform in the Transdanubian Mid-Mountains, Hungary. *Special Publication of the International Association of Sedimentologists*, 19, 303-322.

Haas, J., 2004. Characteristics of peritidal facies and evidences for subaerial exposures in Dachstein-type cyclic platform carbonates in the Transdanubian Range, Hungary. *Facies*, 50(2), 263-286.

Haas, J., and Tardy-Filácz, E., 2004. Facies changes in the Triassic–Jurassic boundary interval in an intraplatform basin succession at Csővár (Transdanubian Range, Hungary). *Sedimentary Geology*, 168, 19–48.

Haq, B., 2018. Triassic eustatic variations reexamined. *GSA Today*, 28, 4-9.

Hay, W.W. and Leslie, M.A., 1990. Could possible changes in global groundwater reservoir cause eustatic sea level fluctuations? In: Geophysics Study Committee, C.o.P.S., Mathematics and Resources, National Research Council, (ed.). *Sea level change*: Studies in Geophysics. National Academy Press, Washington DC, 161–170.

Hinnov, L.A., 2018. Chapter 1: Cyclostratigraphy and Astrochronology in 2018, in Montenari, M., ed., *Stratigraphy and Timescales*, 3, 1-80.

Hinnov, L.A., Ruhl, M., and Hesselbo, S.P., 2018. Reply to the Comment on "Astronomical constraints on the duration of the Early Jurassic Pliensbachian Stage and global climatic fluctuations" [Earth Planet. Sci. Lett. 455 (2016) 149–165]. *Earth and Planetary Science Letters*, 481, 415-419.

Hinnov, L.A., Wu, H., and Fang, Q., 2016. Reply to the comment on "Geologic evidence for chaotic behavior of the planets and its constraints on the third-order eustatic sequences at the end of the Late Paleozoic Ice Age" by Qiang Fang, Huaichun Wu, Linda A. Hinnov, Xiuchun Jing, Xunlian Wang, and Qingchun Jiang [Palaeogeography Palaeoclimatology Palaeoecology 400 (2015) 848–859]. *Palaeogeography Palaeoclimatology Palaeoecology*, 461, 475-480.

Hinnov, L.A., Anastasio, D., Kodama, K., Elrick, M., and Latta, D.J., 2013. Global Milankovitch cycles recorded in rock magnetism of the shallow marine Lower Cretaceous Cupido Formation, northeastern Mexico, in Jovane, L., Herrero-Bervera, E., Hinnov, L.A., and Housen, B., eds., "Magnetic Methods and the Timing of Geological Processes," *Geological Society of London Special Publication*, 373.

Hinnov, L.A., 2000. New perspectives in orbitally forced stratigraphy. *Annual Reviews of Earth and Planetary Sciences*, 28, 419-475.

Hinnov, L.A., and Hilgen, F., 2012. Chapter 4: Cyclostratigraphy and Astrochronology, in Gradstein, F.M., Ogg, J., Schmitz, M., and Ogg, G., eds., *The Geologic Time Scale 2012*, Elsevier, 63-83.

Jacobs, D.K., and Sahagian, D., 1995. Milankovitch Fluctuations in Sea Level and Recent Trends in Sea-Level Change: Ice may not always be the answer. In Haq., B. (ed.), *Sequence Stratigraphy and Depositional Response*

to Eustatic, Tectonic and Climatic Forcing, Kluwer Academic, 329-366.

Kent, D.V., et al., 2018. Empirical evidence for stability of the 405-kiloyear Jupiter–Venus eccentricity cycle over hundreds of millions of years. Proceedings of the National Academy of Sciences, https://doi.org/10.1073/pnas.1800891115.

Kent, D.V., Olsen, P.E., Muttoni, G., 2017. Astrochronostratigraphic polarity time scale (APTS) for the Late Triassic and Early Jurassic from continental sediments and correlation with standard marine stages. *Earth Science Reviews*, 166, 153–180.

Kent, D.V., Olsen, P.E., and Witte, W.K., 1995. Late Triassic-earliest Jurassic geomagnetic polarity sequence and paleolatitudes from drill cores in the Newark rift basin, eastern North America. *Journal of Geophysical Research*, 100, 14,965-14,998.

Kotov, S. and Pälike, H., 2017. Dynamic time warping program to sutomatically tune and correlate stratigreaphical series, 18th *International Association for Mathematical Geosciences Conference*, Perth, Australia, p. 206.

Laskar, J., Robutel, P., Joutel, F., Gastineau, M., Correia, A.C.M. and Levrard, B., 2004. A long-term numerical solution for the insolation quantities of the Earth. *Astronomy and Astrophysics*, 428, 261-285.

Le Tourneau, P. M. and Olsen, P. E. (eds.), 2003. *The Great Rift Valleys of Pangea in Eastern North America*, Volumes 1 and 2, Columbia University Press.

Li, M., Hinnov, L.A., and Kump, L. (2019), Acycle: time-series analysis software for research and education in cyclostratigraphy, *Computers and Geosciences*, 127, 12-22, https://doi.org/10.1016/j.cageo.2019.02.011

Li, M., Hinnov, L.A., Huang, C. and Ogg, J., 2018. Sedimentary noise and sea levels linked to land-ocean water balance dynamics and long-term obliquity forcing, *Nature Communications*, 9, 1004.

Lin, L., Khider, D., Lisiecki, L.E., and Lawrence, C.E., 2014. Probabilistic sequence alignment of stratigraphic records. *Paleoceanography*, 29, 976–989,

Lisiecki, L.E., and Lisiecki, P.A., 2002. Application of dynamic programming to the correlation of paleoclimate records. *Paleoceanography*, 17(4), 1049-

Mandl, G.W., 2000. The Alpine sector of the Tethyan shelf – examples of Triassic to Jurassic sedimentation and deformation from the Northern Calcareous Alps. *Mitteilungen der Österreichischen Geologischen Gesellschaft*, 92 (1999), 61–77.

Mann M.E., and Lees J.M., 1996. Robust estimation of background noise and signal detection in climatic time series. *Climatic Change,* 33, 409-445.

Martini, R., Zaninetti, L., Lathuillière, B., Cirilli, S., Cornée, J.-J., and Villeneuve, M., 2004/ Upper Triassic carbonate deposits of Seram (Indonesia): palaeogeographic and geodynamic implications. *Palaeogeography Palaeoclimatology Palaeoecology*, 206(1-2), 75-102.

Marton, E. and Haas, J., 1996. Ancient platform carbonates with well-developed Lofer cyclicity: new candidates for magnetostratigraphy and geodynamically oriented palaeomagnetism. *Geophysical Journal International*, 126(1), 253-262.

Maurer, F., Rettori, R., and Martini, R., 2008. Triassic stratigraphy, facies and evolution of the Arabian shelf in the northern United Arab Emirates, *International Journal of Earth Sciences*, 97, 765-784.

Mette, W., Thibault, N., Krystyn, L., Korte, C., Clemence, M.-E., Ruhl, M., Rizzi, M., and Ullmann, C.V., 2016. Field Trip 11: Rhaetian (Late Triassic) biotic and carbon isotope events and intraplatform basin development in the Northern Calcareous Alps, Tyrol, Austria, *Geol.Alp*, 13, 233-256.

Mette, W., Elsler, A. and Korte, C., 2012. Palaeoenvironmental changes in the Late Triassic (Rhaetian) of the Northern Calcareous Alps: Clues from stable isotopes and microfossils.

Palaeogeography, Palaeoclimatology, Palaeoecology, 530-352, 62-72.

Meyers, S.R., 2019. Cyclostratigraphy and the problem of astrochronologic testing. *Earth-Science Reviews*, 190, 190-223.

Meyers, S.R., 2015. The evaluation of eccentricity-related amplitude modulation and bundling in paleoclimate data: an inverse approach for astrochronologic testing and time scale optimization. *Paleoceanography*, 30, 1625–1640.

Meyers, S. R., 2014. Astrochron: An R package for astrochronology. [Available at http://cran.r-project.org/package=astrochron]

Meyers, S. R. 2012. Seeing red in cyclic stratigraphy: spectral noise estimation for astrochronology. Paleoceanography, 27, PA3228, https://doi.org/10.1029/2012PA002307

Meyers, S.R., and Malinverno, A., 2018. Proterozoic Milankovitch cycles and the history of the solar system. *Proceedings of the National Academy of Sciences*, 115(25), 6363-6368.

Meyers, S.R., and Sageman, B.B., 2007. Quantification of deep-time orbital forcing by average spectral misfit: *American Journal of Science*, 307, 773–792.

Muller, R.A., and MacDonald, G.J., 2000. *Ice Ages and Astronomical Causes: Data, Spectral Analysis, and Mechanisms*: London, Springer-Praxis, 318 p.

Muttoni, G., Kent, D.V., Jadoul, F., Olsen, P.E., Rigo, M., Galli, M.T., and Nicora, A., 2010. Rhaetian magneto-biostratigraphy from the Southern Alps (Italy): Constraints on Triassic chronology. *Palaeogeography, Palaeoclimatology, Palaeoecology*, 285, 1-16.

Muttoni, G., Kent, D.V., Olsen, P.E., Di Stefano, P., Lowrie, W., Bernasconi, S.M. and Hernandez, F.M., 2004. Tethyan magnetostratigraphy from Pizzo Mondello (Sicily) and correlation to the Late Triassic Newark astrochronological polarity time scale. *Geological Society of America Bulletin*, 116, 1043-1058.

Ogg, J.G., Huang, C., and Hinnov, L.A., 2014. Triassic time scale status: a brief overview, *Albertiana*, 41, 3-30.

Olsen, P.E., 1990. Tectonic, climatic, and biotic modulations of lacustrine ecosystems – examples from Newark Supergroup of eastern North America. In: Katz, B.J. (Ed.), *Lacustrine Basin, Exploration Case Studies and Modern Analogs*. American Association of Petroleum Geologists, Tulsa, OK, 209–224.

Olsen, P. E., 1986. A 40-million year lake record of early Mesozoic orbital climatic forcing. *Science*, 234(4778), 842–848.

Olsen, P.E., 1980. The latest Triassic and Early Jurassic formations of the Newark basin (eastern North America, Newark Supergroup): stratigraphy, structure, and correlation. *New Jersey Academy Sciences Bulletin*, 25, 25-51.

Olsen, P.E., Laskar, J., Kent, D.V., Kinney, S.T., Reynolds, D.J., Sha, J., Whiteside, J.H., 2019. Mapping Solar System chaos with the Geological Orrery. *Proceedings of the National Academy of Sciences*, https://doi.org/10.1073/pnas.1813901116

Olsen, P.E., Geissman, J.W., Kent, D.V., Gehrels, G.E., Mundil, R., Irmis, R.B., Lepre, C., Rasmussen, C., Giesler, D., Parker, W.G., Zakharova, N., Kuerschner, W.M., Miller, C., Baranyi, V., Schaller, M.F., Whiteside, J.H., Schnurrenberger, D., Noren, A., Brady Shannon, K., O'Grady, R., Colbert, M.W., Maisano, J., Edey, D., Kinney, S.T., 2018, Colorado Plateau Coring Project, Phase I (CPCP-I): A continuously cored, globally exportable chronology of Triassic continental environmental change from Western North America. *Scientific Drilling*, 24, 15-40.

Olsen, P.E., Kent, D.V., and Whiteside, J. H., 2011. Implications of the Newark Supergroup based astrochronology and geomagnetic polarity time scale (Newark-APTS) for the tempo and mode of the early diversification of the Dinosauria, *Earth and Environmental Science Transactions of the Royal Society of Edinburgh*, 101, 201-229.

Olsen, P.E., 2010. Fossil Great Lakes of the Newark Supergroup - 30 years later, in Benimoff A.I. (ed.), Field Trip Guidebook, New York State Geological Association, 83nd *Annual Meeting, College of Staten Island*, 101–162.

Olsen, P.E., and Kent, D.V., 1999. Long-period Milankovitch cycles from the Late Triassic and Early Jurassic of eastern North America and their implications for the calibration of the Early Mesozoic time-scale and the long-term behaviour of the planets. Philosophical *Transactions of the Royal Society of London*, Series A, 357, 1761-1786.

Olsen, P.E., and Kent, D.V., 1996. Milankovitch climate forcing in the tropics of Pangea during the Late Triassic. *Palaeogeography, Palaeoclimatology, Palaeoecology,* 122, 1-26.

Olsen, P.E., Kent, D.V., Cornet, B., Witte, W.K., and Schlische, R.W., 1996. High-resolution stratigraphy of the Newark rift basin (early Mesozoic, eastern North America). *Geological Society of America Bulletin*, 108(1), 40-77.

Paillard, D., Labeyrie, L., and Yiou, P., 1996. Macintosh program performs time-series analysis*, Eos,* 77, 379.

Pomoni-Papaioannou, F., Trifonova, E., Tsaila-Monopolis, S. and Katsavrias, N. 1986. Lofer type cyclothems in a Late Triassic dolomitic sequence on the eastern part of the Olympus. *Institute of Geology and Mineral Exploration*, Special Issue, 403–417.

Preto, N., Hinnov, L.A., DeZanche, V., Mietto, P., and Hardie, L.A., 2004. The Milankovitch interpretation of the Latemar platform cycles (Dolomites, Italy): implications for geochronology, biostratigraphy and Middle Triassic carbonate accumulation, in D'Argenio, B., Fischer, A.G., Premoli Silva, I., Weissert, H. and Ferreri, V., eds., Cyclostratigraphy: Approaches and Case Histories, *SEPM Special Publication* No. 81.

Preto, N., and Hinnov, L.A., 2003. Unravelling the origin of carbonate platform cyclothems in the Upper Triassic Dürrenstein Fm. (Dolomites, Italy), *Journal of Sedimentary Research*, 73(5), 774-789.

Preto, N., Hinnov, L.A., Hardie, L.A., and De Zanche, V., 2001. A Middle Triassic orbital signal recorded in the shallow marine Latemar carbonate buildup (Dolomites, Italy). *Geology*, 29, 1123-1128.

Reijmer J.J.G. and Everaars J.S.L., 1991. Carbonate platform facies reflected in carbonate basin facies (Triassic, Northern Calcareous Alps, Austria). *Facies*, 25, 253-278.

Romano, R. Masetti, D., Carras, N., Barattolo, F., and Roghi, G., 2008. The Triassic/Jurassic boundary in a peritidal carbonate platform of the Pelagonian Domain: the Mount Messapion section (Chalkida, Greece). *Rivista Italiana di Paleontologia e Stratigrafia*, 114(3), 431-452.

Samankassou, E. and Enos, P., 2018. Chasing tidal flats in the Triassic of the Austrian Alps to test the "regressive cycles in carbonates" hypothesis of Bob Ginsburg. Abstract, 20th *EGU General Assembly, EGU2018*, Proceedings from the conference held 4-13 April 2018, Vienna, Austria, 15649.

Samankassou, E. and Enos, P., 2017. Lateral variations of carbonate platform facies and cycles: The Dachstein Limestone (Late Triassic, Northern Calcareous Alps, Austria). Abstract, 19th *EGU General Assembly, EGU2017*, proceedings from the conference held 23- 28 April 2017, Vienna, Austria, 16976.

Sander, B., 1951. *Contributions to the study of depositional fabrics: Rhythmically deposited Triassic limestones and dolomites:* American Association of Petroleum Geologists, Tulsa, 207 p. (English translation of Sander, 1936).

Sander, B., 1936. Beiträge zur Kenntnis der Anlagerungsgefüge (Rhythmische Kalke und Dolomite aus der Trias), *Zeitschrift fur Kristallographie, Mineralogie und Petrographie*, I. Nordalpine Beispielen, 48, 27–139.

Satterley A.K. and Brandner R., 1995. The genesis of Lofer cycles of the Dachstein Limestone, Northern Calcareous Alps, Austria. *Geologische Rundschau*, 84, 287-292.

Satterley A.K., 1996. Cyclic carbonate sedimentation in the upper Triassic Dachstein Limestone, Austria: the role

of patterns of sediment supply and tectonics in a platform-reef-basin system. *Journal of Sedimentary Petrology*, 66, 307-323.

Savitzky, A. and Golay, M.J.E., 1964. Smoothing and Differentiation of Data by Simplified Least Squares Procedures. *Analytical Chemistry*, 36(8), 1627-1639.

Schoene, B., Guex, J., Bartolini, A., Schaltegger, U., and Blackburn, T.J., 2010. Correlating the end-Triassic mass extinction and flood basalt volcanism at the 100 ka level. *Geology*, 38, 387–390.

Schwarzacher, W., 2005. The stratification and cyclicity of the Dachstein Limestone in Lofer, Leogang and Steinernes Meer (Northern Calcareous Alps, Austria). *Sedimentary Geology*, 181, 93-106.

Schwarzacher, W., 1954. Die Grossrhythmik des Dachsteinkalkes von Lofer. *Tschermaks Mineralogische und Petrographische Mitteilungen*, 4, 44–54.

Schwarzacher, W., 1947. Über die sedimentäre Rhythmik des Dachsteinkalkes von Lofer. *Verhandlung der Geologische Bundesanstalt*, 10-12, 175–188.

Schwarzacher W., and Haas J., 1986. Comparative statistical analysis of some Hungarian and Austrian Upper Triassic peritidal carbonate sequences. *Acta Geologica Hungarica*, 29, 175-196.

Scotese, C.R., 2013. PALEOMAP PaleoAtlas for ArcGIS, volume 3, Triassic and Jurassic Paleogeographic, Paleoclimatic and Plate Tectonic Reconstructions, PALEOMAP Project, Evanston, IL, https://doi.org/10.13140/2.1.2124.1124

Smoot, J., 2010. Chapter A: Triassic depositional facies in the Newark Basin, in Herman, G.C., and Serfes, M.E. (eds.), Contributions to the Geology and Hydrogeology of the Newark Basin, *New Jersey Geological Survey Bulletin*, 77, A1-A110.

Smoot, J.P., 1991. Sedimentary facies and depositional environments of early Mesozoic Newark Supergroup basins, eastern North America. *Palaeogeography, Palaeoclimatology, Palaeoecology*, 84, 369-423.

Thomson, D.J., 1982. Spectrum estimation and harmonic analysis. *Proceedings of the IEEE*, 70, 1055-1096.

Trauth, M.H., and Sillmann, E., 2018. *Collecting, Processing and Presenting Geoscientific Information*, MATLAB® and Design Recipes for Earth Sciences – Second Edition. Springer Verlag, 274 p.

Van Houten, F.B., 1962. Cyclic sedimentation and the origin of analcime-rich upper Triassic Lockatong Formation, west-central New Jersey and adjacent Pennsylvania. *American Journal of Science*, 260, 561–576.

Van Houten, F.B., 1964. Cyclic lacustrine sedimentation, Upper Triassic Lockatong Formation, Central New Jersey and adjacent Pennsylvania. In: Merriam, D.F. (ed.), Symposium on Cyclic Sedimentation, *Kansas Geological Survey Bulletin*, 169, 497–531.

Waltham, D., 2015. Milankovitch period uncertainties and their impact on cyclostratigraphy. *Journal of Sedimentary Research*, 85, 990-998.

Wagreich, M., Lein, R. and Sames, B., 2014. Eustasy, its controlling factors and the limno-eustatic hypothesis—concepts inspired by Eduard Suess. *Austrian Journal of Earth Sciences,* 107, 115-131.

Wendler, J. E., Wendler, I., Vogt, C. and Kuss, J., 2016. Link between cyclic eustatic sea-level change and continental weathering: Evidence for aquifer-eustasy in the Cretaceous. *Palaeogeography, Palaeoclimatology, Palaeoecology*, 441, 430–437.

Withjack, M.O., Schlische, R.W., Malinconico, M.L., and Olsen, P.E., 2013. *Jurassic Newark Basin of eastern North America Rift-basin development: lessons from the Triassic.* Geological Society, London, Special Publications, 369, 301–321.

Withjack, M.O., Schlische, R.W. and Olsen, P.E., 2012. Development of the passive margin of eastern North America: Mesozoic rifting, igneous activity, and breakup. In: Bally, A.W. and Roberts, D.G. (eds), *Regional Geology and Tectonics: Phanerozoic Rift Systems and Sedimentary Basins*. Elsevier, Amsterdam, 300–335,

Wotzlaw, J.-F., Guex, J., Bartolini, A., Gallet, Y., Krystyn, L., McRo42, 571-574, berts, C.A., Schoene, B., and Schaltegger, U., 2014. Towards accurate numerical calibration of the Late Triassic: High precision U-Pb geochronology constraints on the duration of the Rhaetian. Geology, 47, 571-574.

Zaffini, M., Jadoul, F., and Rigo, M., 2018. A new Rhaetian $\delta^{13}C_{org}$ record: Carbon cycle disturbances, volcanism, End-Triassic mass Extinction (ETE). *Earth-Science Reviews,* 178, 92-104.

Zühlke, R., 2004. Integrated cyclostratigraphy of a model Mesozoic carbonate platform—the Latemar (Middle Triassic, Italy), in D'Argenio, B., Fischer, A.G., Premoli Silva, I., Weissert, H. and Ferreri, V., eds., *Cyclostratigraphy: Approaches and Case Histories*, SEPM Special Publication No. 81, 167-182.

Recibido: julio 2019
Revisado: noviembre 2019
Aceptado: enero 2020
Publicado: marzo 2021